TÉCNICO LISBOA

Extension of communication aeronautical services coverage over the ocean via antenna optimization

Cristina Santos Nobre Dias

Thesis to obtain the Master of Science Degree in

Electrical and Computer Engineering

Supervisor: Prof. Luís Manuel de Jesus Sousa Correia

Examination Committee

Chairperson: Prof. José Eduardo Charters Ribeiro da Cunha Sanguino

Supervisor: Prof. Luis Manuel de Jesus Sousa Correia

Members of Committee: Prof. Custódio José Oliveira Peixeiro

Eng. Luis Rodrigues

December 2017

To my beloved family and friends,

"I now knew that all my anticipations had been justified. I now felt for the first time absolutely certain that the day would come when mankind would be able to send messages around the world, not only across the Atlantic, but between the furthermost ends of the earth" - Marconi

Acknowledgements

Firstly, my sincere gratitude goes to Prof. Luís M. Correia, my thesis supervisor, for giving me the opportunity to work on this master thesis as well as for all the advices, guidance and consideration in our weekly meetings.

I also have to thank the engineers from NAV Portugal, Engs. Carlos Alves, Luis Pissarro and Luis Rodrigues for all the meetings, feedbacks, sympathy. A special thank you for Eng. Luis Rodrigues for all the emails exchange that were essential to the development of this work.

Also, a big thank you to all my colleagues that turned into great friends, who were valuable for my success and conclusion of this chapter of my life, and most important to my family for all the support, for never letting me give up and for always showing my worth, and to Hugo Martins for all the help, for all the patience and motivation, but most crucially, for making me a better student and a better person who is now ready for new chapters of her life.

Thank you all, I really appreciated it!

Abstract

Aeronautical communications are based on ground transmitting/receiving antennas, with a given range, delimited by transmission powers, among other aspects. For routes in transcontinental flights over large oceanic paths, coverage problems may exist, given the large distances that the aircraft may be from ground stations, creating communication problems. The use of multi-frequency systems and directional antennas can contribute to minimize this problem, by extending coverage from the ground station, since it is not possible to act on the aircraft one. For given flight routes, radiation patterns for ground stations can be optimised with directional antennas, from which actual commercial antennas can be deployed. To address this problem, high directive antennas Yagi Uda Antennas radiation patterns were analysed in order to extend the voice communication coverage over the ocean and a suggestion of the location of the ground station, in Azores. Ones conclude that an 18 elements' Yagi antenna, with a maximum forward gain of 16.35 dBi, can extend, in the direction of maximum propagation, about 7% comparing with the current omnidirectional array with 2.5 dBi of gain. In terms of coverage area, some part of the Azores' FIR can be covered using only 18 elements' Yagi antennas, covering approximately 46.05% of the FIR, which corresponds in an improvement of approximately 3% comparing with the current coverage area.

Keywords

Aeronautical Voice Communication; VHF Propagation; Coverage Extension; Radiation Patterns; Yagi Antennas; Multi-frequency Systems.

Resumo

Comunicações aeronáuticas são baseados em antenas transmissoras / receptoras na Terra delimitadas por potências de transmissão, entre outros aspectos. Em casos de voos transcontinentais, que cobrem vastas áreas oceânicas, podem existir problemas de cobertura uma vez que a aeronave pode estar demasiado longe da estação terrestre impossibilitando a comunicação. De modo a minimizar o problema, podem ser utilizadas antenas direcionais conjuntamente com sistemas de multifrequência podendo, portanto, estender a comunicação. Como tal, e uma vez que é impraticável mudar as antenas de todas as aeronaves, para abordar este problema, analisaram-se as antenas bastante directivas, de modo a estender a cobertura de comunicação de voz no oceano. Posteriormente, há uma analise das possíveis localizações das estações terrestres, nas diferentes ilhas dos Açores e posteriormente uma sugestão para a extensão da cobertura com antenas Yagis de 18 elementos. Concluindo, e em termos de direcção de máxima propagação, estas antenas, comparadas com as que se encontram fixadas nos Açores, contribuem para uma extensão do sinal de aproximadamente 7%. Já em termos de área, a extensão é de aproximadamente 3%, cobrindo, portanto, aproximadamente 46.05% de toda a FIR.

Palavras-chave

Comunicação Aeronáutica por Voz; Propagação em VHF; Extensão da Cobertura; Diagramas de Radiação; Antenas Yagi; Sistemas de multifrequência

Table of Contents

Acknowledgements v

Abstract vii

Resumo ix

List of Figures xii

List of Tables xiv

List of Acronyms xv

List of Symbols xvii

List of Software xx

1 Introduction 1

1.1 Overview 2

1.2 Motivation and Contents 4

2 Fundamental concepts and state of the art 7

2.1 VHF Aeronautical Mobile Communication 8

2.2 Propagation models 9

2.3 Antennas for Aeronautical Communications 18

2.4 State of the Art 20

3 Models and simulator description 23

3.1 Model Development 24

3.1.1 Model Overview 24

3.1.2 Propagation Models 25

3.2 Model Implementation 28

3.2.1 Propagation Models 28

3.2.2 Radiation pattern 33

3.3 Model Assessment 37

4 Analysis of Results 45

4.1 Actual coverage scenario 46

4.2 Coverage Improvement 48

4.3 Antennas' Dimension 57

5 Conclusions 59

Annex A. Antennas' Datasheets 63

References 71

List of Figures

Figure 1-1: Aeronautical voice communication (extracted by [2]). 3
Figure 1-2: Lisbon and Santa Maria FIRs (extracted from [4]). 3
Figure 1-3: Communication between pilot and controller with help of satellite (extracted from [6]). 4
Figure 1-4: Backhaul interconnection between mobile ground stations and the core parts of a mobile network ground infrastructure (extracted from [6]). 5
Figure 1-5: VHF radiowave link between the ground station and the airborne antenna (extracted from [6]). 5
Figure 2-1: Typical coverage topology for upper and lower airspaces (extracted from [6]). 9
Figure 2-2: Diagram of Flat Earth Model (extracted from [33]). 10
Figure 2-3: Knife-edge model geometry (extracted from [10]). 11
Figure 2-4: The Spherical Earth Model and the Flath Earth equivalent parameters (extracted from [33]). 11
Figure 2-5: Definition of penumbra width (extracted from [13]). 13
Figure 2-6: Propagation mechanisms: Line-of-sight, Diffraction and Troposcatter (extracted from [13]). 13
Figure 2-7: Profile of a typical troposcatter path (extracted from [15]). 15
Figure 2-8: Refractivity profiles showing surface-based duct (extracted from [18]). 17
Figure 2-9: Curacao Flight Information Region. 21
Figure 2-10: RCAG stations in India (extracted from [29]). 21
Figure 3-1: Model Overview. 24
Figure 3-2: Simulator Overview 29
Figure 3-3: Flowchart of the PrM Simulator with the steps required to estimate radio coverage 29
Figure 3-4: Flow chart for the Deygout/Knife-Edge Model. 30
Figure 3-5: Flowchart for the bellow the horizon algorithm. 30
Figure 3-6: Flowchart for the over-the-horizon algorithm. 31
Figure 3-7: Flowchart of the received power estimation algorithm. 31
Figure 3-8: Approximated estimation of the total coverage representation. 32
Figure 3-9: Total area coverage estimation. 32
Figure 3-10: Definitions for the interpolation method of the 3-D radiation pattern (extracted from [33]). 33
Figure 3-11: Mapping of the sphere's surface onto a planar surface (extracted from [33]). 34
Figure 3-12: Azimuth angle representation. 34
Figure 3-13: Aircraft's fuselage transversal cut showing transponder antennas locations (extracted from [30]). 35
Figure 3-14: Representation of the aircraft's antenna near-field (extracted from [30]). 36
Figure 3-15: Average absolute transponder antenna gain, with 2.25 dBi average standard deviation (extracted from [30]). 36
Figure 3-16: Radio line-of-sight assessment with a considerable obstacle. 38
Figure 3-17: Radio line-of-sight assessment without any considerable obstacle. 38
Figure 3-18: Path Loss for different propagation mechanisms. 39
Figure 3-19: Horizontal and Vertical Cuts of the SC272 Omnidirectional Array interpolated gain (G_{max}=2.15 dBi). 41

Figure 3-20: Horizontal and Vertical Cuts of the Yagi 3 elements' interpolated gain (G_{max}=7.8 dBi). 41
Figure 3-21: 3D representation of the interpolated gain for the Yagi 3 elements' Antenna. 41
Figure 3-22: 3D representation of the interpolated gain for the SC272 Omnidirectional array... 42
Figure 3-23: Power Assessment- GS as Receiving Antenna..... 42
Figure 3-24: Power Assessment- Aircraft as Receiving Antenna. 43
Figure 3-25: Estimated coverage of Azores' FIR given by NAV Portugal (adapted from [4]). 43
Figure 3-26: Estimated coverage of Azores' FIR given by the simulator. 44
Figure 3-27: Comparison of the coverage estimated by the simulator and the one given by NAV..... 44
Figure 4-1: Locations of the GSs in Azores' FIR. 46
Figure 4-2: Elevation plane pattern for the aircraft. 47
Figure 4-3: Representation of overlapping coverage for aeronautical communication services. 48
Figure 4-4: E and H-Plane for Yagi 6 elements' antenna. 49
Figure 4-5: 3D interpolated Radiation pattern for Yagi 6 elements' antenna. 49
Figure 4-6: E and H-Plane for Yagi 12 elements' antenna. 49
Figure 4-7: 3D interpolated Radiation pattern for Yagi 12 elements' antenna. 50
Figure 4-8: E and H-Plane for Yagi 18 elements' antenna. 50
Figure 4-9: 3D interpolated Radiation pattern for Yagi 18 elements' antenna. 50
Figure 4-10: Path representation to analyse the coverage length in Morro Alto, Flores. 51
Figure 4-11: Coverage for each antennas' type when the aircraft is flying South->North (FL245). 51
Figure 4-12: Aircraft's route flying from West to East. 52
Figure 4-13: Coverage for each antennas' type when the aircraft is flying West>East (FL245). 52
Figure 4-14: Coverage for each antennas' type when the aircraft is flying South->North (FL400). 53
Figure 4-15: Direction of orientation of the 18 elements' Yagi antennas in the GSs (adapted from [38]). 54
Figure 4-16: Propagation coverage area when using Yagi 18 elements' antennas in the GS (FL245). 54
Figure 4-17: Comparison between the improved and the actual coverages. 55
Figure 4-18: 18 elements' Yagi directions of orientation for the 4-frequency system (adapted from [38]). 55
Figure 4-19: Testing aircraft's route from NE heading SW for the Morro Alto, Flores, Ground Station. 56
Figure 4-20: Comparison of coverage maximum distances when the aircraft's route goes from NE to SW using 18 elements' Yagi pointing north and pointing SW. 56
Figure 4-21: Coverage in case of having 4 working frequencies. 57
Figure A-1: Sinclair's omnidirectional array SC6172 elevation pattern (extracted from [40]). 64
Figure A-2: Sinclair's Omnidirectional SC272 Array Elevation Pattern (extracted from [40]). ... 65
Figure A-4: 6 elements Yagi Antenna's Free Space Radiation Patterns (extracted from [35])...66
Figure A-5: 12 elements Yagi Antenna's Free Space Radiation Patterns (extracted from [36]).67
Figure A-6: 18 elements Yagi Antenna's Free Space Radiation Patterns (extracted from [37]).68

List of Tables

Table 3.1: Validation of the simulator. 37
Table 3.2: Parameter assumptions. 37
Table 3.3: Numerically calculated parameters. 40
Table 4.1: Information about the VHF ground station antennas of NAV. 46
Table 4.2: Heights of the terrain profile and consequently, of the GSs above mean sea level. . 47
Table 4.3: Comparison between the maximum distance for each antenna's type for FL245 and FL400. 53
Table 4.4: Comparison between the current and the improved coverage area. 55
Table 4.5: Total coverage improvement for 4-frequency system. 56
Table 4.6: Reflector and directors' dimensions for the 18 elements' Yagi in the Airband. 58
Table 4.7: Reflector and directors' dimensions for the 6 elements' Yagi in the Airband. 58
Table A.1: Sinclair's Omnidirectional Array SC6172 Specifications (extracted from [40]). 64
Table A.2: Sinclair's Omnidirectional Array SC272 Specifications (extracted from [40]). 65
Table A.3: 3 elements Yagi Antenna's Specifications (extracted from [34]). 66
Table A.4: 6 elements Yagi Antenna's Specifications (extracted from [35]). 67
Table A.5: 12 elements Yagi Antenna's Specification (extracted from [36]). 68
Table A.6: 18 elements Yagi Antenna's Specifications (extracted from [37]). 69

List of Acronyms

A3E	Double Sideband Amplitude Modulation for Analog Communication
AM	Amplitude Modulation
AM(R)S	Aeronautical Mobile (Route) Service
ANSP	Air Navigation Service Provider
ASTER GDEM V2	Advanced Spaceborne Thermal Emission and Reflection Radiometer Global Digital Elevation Model Version 002
ATC	Air Traffic Control
DSB-AM	Double Side Band in Amplitude Modulation
DSB-FC	A3E double sideband with full carrier
EGM96	Earth Gravitational Model
EIRP	Equivalent Isotropically Radiated Power
FIR	Flight Information Region
FL	Flight Level
FM	Frequency Modulation
GDEx	Global Data Explorer
GeoTIFF	Geographic Tagged Image File Format
GS	Ground Station
HF	High Frequency
ICAO	International Civil Aviation Organization
ITU	International Telecommunications Union
ITU-R	International Telecommunications Union – Radio sector
LOS	Line-of-Sight
LP DAAC	Land Processes Distributed Active Archive Centre
MDS	Minimum Discernible Signal
METI	Japan’s Ministry of Economy, Trade, and Industry
MSL	Mean Sea Level
NASA	U.S. National Aeronautics and Space Administration
NAV Portugal, EPE	Navegação Aérea de Portugal
PrM	Propagation Model

PTT	Push-To-Talk
SATCOM	Satellite Communication
SATVOICE	Satellite Voice System
TMA	Terminal Manoeuvring Area
UARs	Upper Air Routes
UHF	Ultra-High Frequency
UNICOM	Universal communications
VHF	Very High Frequency
WGS84	1984 World Geodetic System
WRC	World Radio Conference

List of Symbols

λ	Wavelength of the transmitted signal
λ_A	t^{th} geodetic longitude sample along a great circle arc
Δd_{DEM}	Sampling resolution of the terrain profile
Δh_{duc}	Height of top of duct above transmitting antenna.
Δh_{GS}^{A}	Difference between aircraft and Ground stations height
ΔP_r	Power above the Sensitivity
$\Delta\theta_c$	Sampling resolution of the geocentric angle
$\Delta\phi$	Phase difference between using the Flat Earth and Spherical Earth Models
β	Parameter allowing for the type of ground
σ	Electrical conductivity
θ	Angle between the vertical plane and the beam direct
θ_A	Polar angle on the aircraft
θ_{GS}	Polar angle on the ground stations antennas
θ_c	Geocentric angle between the Ground station and the aircraft
θ_t	Horizon angle at the transmitter
θ_r	Horizon angle at the receiver
ϕ	Angle between the horizontal plane and the beam direct
ϕ_A	Geodetic latitude of the aircraft
$\Phi_{A-GS,t}$	t^{th} geodetic latitude sample along a great circle arc
ϕ_{GS}	Geodetic latitude of the Ground Station
Ψ_{A-BS}	Azimuth of the great circle arc at the aircraft location
δ	Electric phase difference between the N^{th} antenna and the reference one
γ	Atmospheric structure parameter
γ_{del}	Phase delay
d	Radio-path length
d_a	Ground distance between the aircraft and the reflection point
d_{ant}	Distance between the dipoles
d_r	Distance from the obstacle to the receiver

d_{RH}	Distance from the terminal to its radio horizon
d_s	Ground distance between the station and the reflection point
d_t	Distance from the obstacle to the transmitter
E	Diffraction field strength
E_o	Free-space field strength
E_r	Electric Field Strength in the receiving antenna
$E_{r,min}$	Receiver Electric Field Sensitivity
f	Frequency
F_{aa}	Antenna's array factor
$G_{antenna}$	Gain of the array antenna element
G_{GS}	Interpolated GS gain
$\mathrm{G_{max}}$	Maximum Gain
G_t	Transmitting antenna gain
G_r	Receiving antenna gain
$h_{A,MSL}$	Aircraft height above mean sea level
$h_{GS,MSL}$	Ground station height above mean sea level
$h_{ef,A}$	Equivalent effective height of the aircraft in the Flat Earth model
$h_{ef,GS}$	Equivalent effective height of the terminal in the Flat Earth model
h_r	Height of the receiver
h_t	Height of the transmitter
$h_{t,MSL}$	Height above Mean Sea Level (MSL) of the terminal
h_{ofe}	Height from the tip of obstacle to the centre of the ellipsoid
k	Earth's Multiplication factor
L	Length of the dipole
L_C	Aperture-to-medium coupling loss
L_{dif}	Total path loss for a distance d due to diffraction by Earth's Curvature
L_{fs}	Total path Loss
L_{KE}	Additional path loss from considerable obstacles
L_p	Total path loss
$L(q)$	Average annual median transmission loss
n	Order of the Fresnel Ellipsoid
N_{ant}	Number of elements in the array

P_{EIRP}	Equivalent isotropic radiated power
P_r	Received Power
$P_{r,min}$	Lowest power level at which the receiver can detect an RF signal
P_t	Power fed to the transmitting antenna
r_A	Effective distance of the aircraft's antenna to the Earth's centre
r_{GS}	Effective distance of the ground station's antenna to the Earth's centre
R	Earth's Radius
R_e	Effective Earth's radius
$R_{f\,e,n}$	Radius of the Fresnel Ellipsoid of order n
S	Percentage of coverage area
ν	Obstacle impediment coefficient
W	Penumbra width
X	Normalized length of the path between the antennas
Y_1	Transmitter normalized height
Y_2	Receiver normalized height
$Y(q)$	Conversion factor for non-exceedance percentages q other than 50%

List of Software

Adobe Photoshop CC 2016	Raster graphics editing software
Draw.io	Flowcharts Marker and Diagram Online Software
Google Earth	Map and geographical information software
MATLAB R2016a	Numerical simulation software
Microsoft Excel 2016	Spreadsheet software
Microsoft Word 2016	Word processor software

Chapter 1

Introduction

This chapter gives the context of the study in nowadays' systems. In order to understand better the relevance of the work, a brief overview is given, as well its impact in the area of study. It is finalised with a brief presentation of the structure of this study.

1.1 Overview

Before radio was available for aeronautical communications and for pilots to warn the control tower that they were about to land, pilots dipped a wing and that signal was often misinterpreted. Also, controllers communicated with coloured light guns, each colour representing a message. The wing dipping continued until early 1930s when the first radios on-board were installed on aircrafts at a larger scale, but only in 1940s radios became generally available for use on all aircrafts worldwide.

It is stated in [1] that the modern system of air traffic control (ATC) was born at the Cleveland Airport in Ohio, where a control tower was constructed on top of an old hangar and equipped with radio transmitting and receiving equipment. Communication transmitters were 15 W radios that allowed voice communication with pilots over approximately 24 km. Using this primitive radio equipment, the air traffic controller could communicate directly with the pilots of the properly equipped aircraft. In addition, the pilots could respond to these instructions or initiate communication. For the airborne that were not radio equipped the control tower was still equipped with light guns, and the light guns were also used for backup communications in case of radio equipment malfunction in either the control tower or the aircraft.

At first, communication was only made in high frequency (HF) bands or even in medium frequencies, prone to static and atmospheric noise, but not for a long time. Air-ground communications relied upon very high frequencies (VHF) due to its high-quality capability of transmitting voice in very high ranges, limited by the elevation of the ground station, the altitude of the aircraft and the ground topology between the two. For high-flying aircrafts, the range could go up to 300 NM.

International Civil Aviation Organization (ICAO), formed in April 1947, soon recognized that a more structured approach to aeronautical communications was required. In parallel to the formation of ICAO, and due to its growing influence, the VHF [118, 132] MHz band was designated for aeronautical communications by the World Radio Conference (WRC) in Atlantic City in 1947, with the advent of the Aeronautical Mobile (Route) Service (AM(R)S). The AM(R)S, by definition, is “a service reserved for communication relating to the safety and regularity of flight, primarily along national or international civil air routes”.

Firstly, the AM(R)S system used Double Side Band in Amplitude Modulation (DSB-AM), mainly due to its simplicity and resilience in the environment, with 200 kHz channel spacing, accommodating 70 channels over the whole band. Then, in 1950, to double the capacity to 140 channels, channel spacing changed to 100 kHz. At the same time, an extension of the band was allocated for AM(R)S to [118, 136] MHz, increasing the number of channels to 180.

Ten years later, this methodology was extended further with 50 kHz channel spacing, now easily achievable, and this doubled the capacity again to 360 channels at the rate of 50 kHz. Finally, in 1972, 25 kHz channel spacing was introduced with theoretical 720 channels. However, that was not enough to curb demand. Therefore, in 1979, WRC extended the AM(R)S allocation in the VHF band even more to [117.975, 137.000] MHz, which is the current situation today, with a theoretical 760 channels at the rate of 25 kHz achievable.

In domestic airspace, flight information is typically transmitted and received using VHF and Ultra-High Frequency (UHF) voice radio whereas their propagation is limited by the radio horizon. Places not covered by either VHF or UHF must be covered by HF radio and/or by satellite voice systems (SATVOICE).

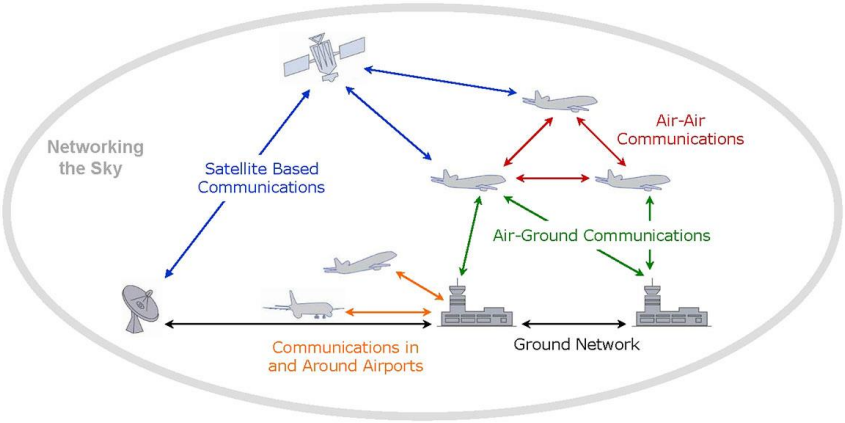

Figure 1-1: Aeronautical voice communication (extracted by [2]).

Every flight must be supervised by an entity that manages air traffic. In Portugal, there are two Flight Information Regions (FIR) that are controlled by an Air Navigation Service Provider (ANSP), which oversees, controls and assists the departure and arrival of aircrafts, and maintains secure traffic throughout the airspace. As stated in [3], NAV Portugal is the Portuguese ANSP, being responsible for both the Santa Maria and Lisbon FIRs, Santa Maria being one of the largest FIRs located in the Atlantic Ocean, as shown in Figure 1-2.

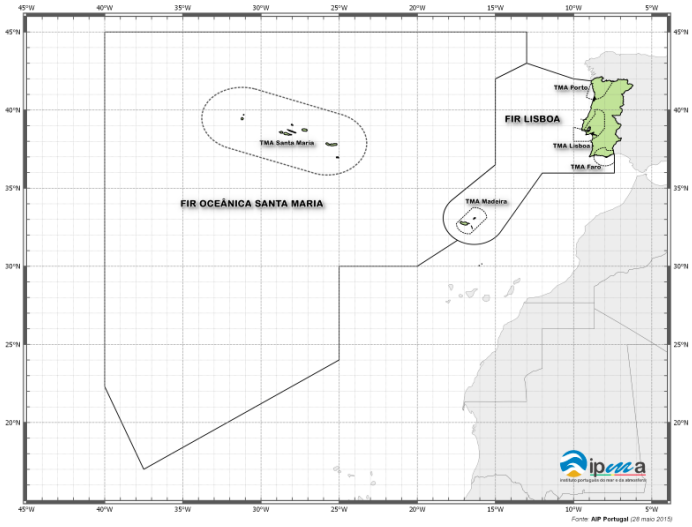

Figure 1-2: Lisbon and Santa Maria FIRs (extracted from [4]).

These centres carry out the approach control for the Lisbon, Porto, Faro, Funchal and Porto Santo airports in the Lisbon FIR, and in the Azores airports under the Oceanic FIR. Alongside the Ocean

Control Centre in Santa Maria, there is a modern communications centre that ensures effective long-distance coverage, using an HF system, since this is an Oceanic FIR.

1.2 Motivation and Contents

The very first aeronautical frequencies used for communications were HF, for two reasons. First, the equipment was easy to make, with reasonably high-power amplifiers, and secondly, the antenna systems were, and still are today, highly efficient, so that most of the power being launched goes into the radio beam. Even though, the HF band has the possibility of propagate the signal thousands of kilometres, through the ionosphere, in some cases even curve around a significant part of the earth's globe, with low reflections losses, it can also be a problem. In fact that is very common, since unwanted radio waves can equally propagate a long way, resulting on a build-up or aggregation of unwanted signals, causing interference and lifting the noise floor whereas comparing the VHF with the HF, the link quality is much better and there is greater reuse of the frequency channel.

In domestic airspace, to send/receive flight information UHF voice radios is also used. In UHF, radio waves propagate almost entirely by line-of-sight and ground reflection. They are blocked by hills and cannot travel far beyond the horizon. For long distances suffer attenuation due to the atmospheric moisture, whereas VHF propagation is less affected.

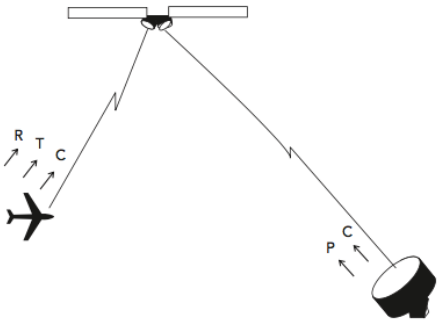

Figure 1-3: Communication between pilot and controller with help of satellite (extracted from [6]).

In cases where VHF coverage does not exist and HF communications fails, aircrafts use satellite communication (SATCOM) for ATC communications (Figure 1-3). Aircrafts have been able to carry out voice via the Inmarsat satellites for more than 25 years.

Currently, the number of aircrafts equipped to use Inmarsat has exceeded 3,500, and is made up of airliners, business jets, and government aircraft. There are four satellites placed in geo-stationary orbit above the equator, centralized over the four oceans - Pacific Ocean, Indian Ocean, Atlantic Ocean-East, and Atlantic Ocean-West – providing coverage through a "global beam" between 80º above and below the equator. SATCOM can provide reliable, high quality communications, but with the advantage of a relatively higher cost of service provision. For these reasons, engineers have expended much effort developing and refining VHF radio technology to communicate beyond the horizon.

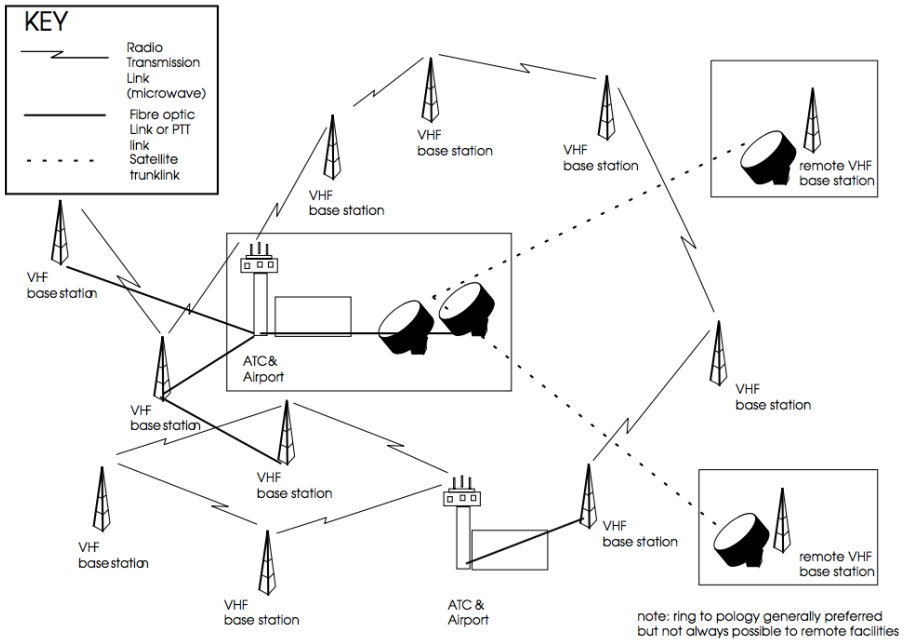

Figure 1-4: Backhaul interconnection between mobile ground stations and the core parts of a mobile network ground infrastructure (extracted from [6]).

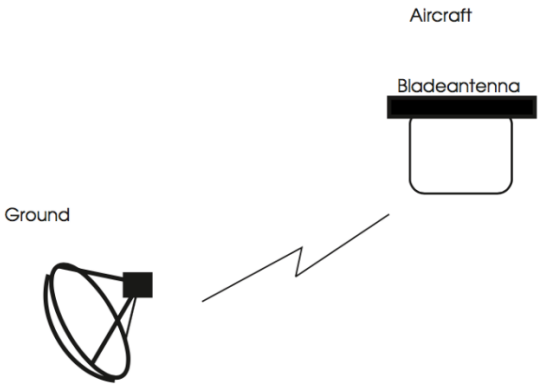

Figure 1-5: VHF radiowave link between the ground station and the airborne antenna (extracted from [6]).

En-route air traffic controllers work in ATC, Figure 1-4. Each centre is responsible for many thousands of square miles of airspace (FIRs) and for the airports within that airspace. The pilot communicates with the controller through one of the VHF ground stations in the network. To avoid interferences, close by VHF ground stations are normally tuned with different frequencies. Neighbouring the ATC, there are one or more ground stations linked normally by optical fibres. These antennas send the information, through radio transmission or, in case of the remote VHF ground stations by satellite, which subsequently is received by the aircrafts' antennas (Figure 1-5).

The problem is that normally these VHF ground station antennas are omnidirectional with small gains. So, this thesis, which was made in collaboration with NAV Portugal, is precisely motivated by extending

coverage beyond the horizon where a model for optimised antenna radiation patterns was developed by multi-frequency systems, in the Azores.

The thesis is divided into a total of 5 chapters, including the present introductory one, and it is complemented with 1 annex with information about the antennas studied for this work.

In Chapter 2, one begins by presenting how aeronautical voice communications works, following the theoretical propagation models for short and long distances, and afterwards techniques to increase and improve coverage for aeronautical purposes. In the end, the state of the art regarding the focus of this thesis is briefly presented.

Chapter 3 details with flowcharts the model implementation, as well as the assessment to the simulator in order to extend the coverage area of Azores' FIR, and Chapter 4 presents the description of the scenarios for performance analysis. Furthermore, there is also the study of high gain Yagi antennas with the purpose of covering distances longer than the ones already obtained, as well as the study of their location and to where they are pointed to.

Finally, Chapter 5 concludes the thesis highlighting the main results of this work and presenting relevant conclusions about each chapter.

At the end, there is, in the annex, information related to the omnidirectional arrays as well as the 6, 12 and 18 elements' Yagi antennas datasheets.

Chapter 2

Fundamental concepts and state of the art

This chapter provides an overview of aeronautical voice communication, its propagation models and ways of improving/extending VHF coverage.

2.1 VHF Aeronautical Mobile Communication

This section contains information about voice communication in VHF between ground station and aircraft, based on [7], [6] , [8], and [9].

A satisfactory fact about VHF is that it is a line of sight system, which for an aircraft flying at sufficient height gives sufficient signal from the ground and to the ground controller. As the aircraft passes from one transmitter to another, typically they need to retune, since neighbouring transmitters are normally set to different frequencies.

Mainstream civil aeronautical communications in VHF band uses the frequency band [117.975, 137.000] MHz, named as Airband or Aircraft band. Control towers use the [118.000, 121.400] MHz band to communicate with the aircraft, and [121.600, 122.900] MHz is used for ground and apron control. The air-to-air universal communications (UNICOM) frequency is 123.450MHz, and [124.000, 128.800] MHz is used for arrivals and departures. En-route area control centre communication uses the [132.000, 135.975] MHz band.

Communication between the pilot and the controller on the ground normally is via VHF analogue voice radio, where one channel is assigned to an ATC. If the aircraft is getting closer to that sector, the pilot tunes the radio to the channel assigned to the sector.

When a message needs to be transmitted, by the pilot or the controller, they must listen first to the channel to see if it is busy and, if so, wait for a quiet period in the traffic on that channel. Normally the waiting period is relatively short, because, for most channels, transmissions are short and traffic is light. For highly-congested channels, the wait can be 30 s or more. With judgement and experience, the pilot/controller presses the push-to-talk (PTT) switch and states his/her message, as fast and succinct as possible, to minimize channel occupancy. Then, the sender listens to the channel until he/she receives acknowledge that the message was sent successfully. In case of failure, it means that two transmitters were activated at the same time and both failed to communicate or the receiver failed to listen the message. Therefore, a new message should be sent.

As stated above, worldwide aircraft communication radio operations use amplitude modulation, predominantly A3E double sideband with full carrier (DSB-FC) on VHF. For audio communication, conventional amplitude modulation (AM) is used with channel spacing of 25 kHz (760 channels) or in 8.33 kHz spacing (theoretically 2 280 channels), although the latest is not going to be considered. It is worth noting that even though frequency modulation gives higher speech quality, it is not typically used, since it covers a 300 kHz bandwidth, and that speech quality is not required.

Double sideband with amplitude modulation (DSB-AM) is very easy to work with, power-efficient and compatible with other equipment. Also, it allows stations with stronger signals to overtake weaker stations, or suffering interference, and does not suffer from the capture effect found in frequency modulation (FM) (which only the stronger of two signals at, or near, the same frequency will be demodulated). In case of both pilot and the control tower are transmitting at the same time, other aircraft will hear a mixture of both transmissions, instead of just one of them.

2.2 Propagation models

This section contains information about the transmission links between ground station and aircraft, based on [10], [11], [12] and [13].

In generic mobile systems, a coverage area is typically split into rural, sub-urban or urban areas. In aeronautical equivalent these terms are en-route coverage, terminal manoeuvring area (TMA) coverage, and local airport coverage. Also, the airspace can be divided in upper and lower ones. The separation between the two happens at flight level (FL) 245 (approximately an altitude of 7 450 m). Far away from the TMA, aircrafts usually fly at FL300 or higher:

- For upper airspace, the coverage can be assumed limited, in LOS links, by the horizon and link budget considering the curvature of the Earth with a conservative factor of *k* equal to 4/3.
- For ground links and low-airspace links, the terrain, building clutter and other likely obstruction should be carefully studied by the Fresnel's first Ellipsoid.

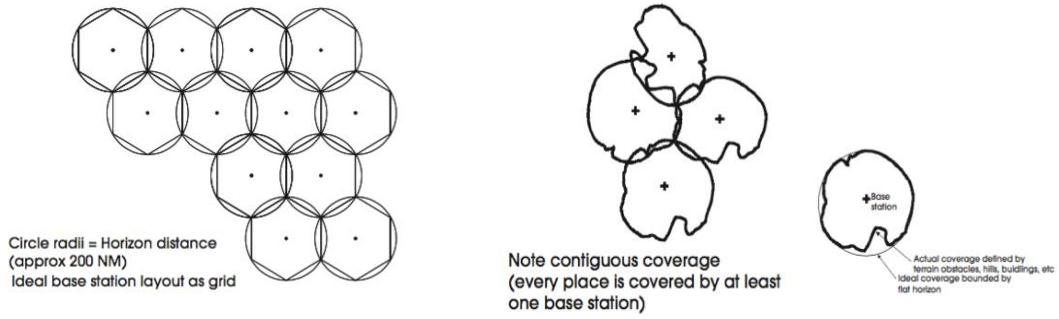

(a) Upper airspace (b) Lower airspace

Figure 2-1: Typical coverage topology for upper and lower airspaces (extracted from [6]).

For short communication between two links, with no obstacles between them, the total path loss is limited to the free space path loss, which can be calculated by [10]:

$$L_{fs[\mathrm{dB}]} = 32.5 + 20\log_{10} d_{[\mathrm{km}]} + 20\log_{10} f_{[\mathrm{MHz}]} \quad (2.1)$$

where:

- d is the distance between the transmitting and the receiving antennas;
- f is the frequency of the signal.

Also, the effect of the Earth's curvature is negligible for short distances, so the Flat Earth propagation model can be use. Figure 2-2 depicts the transmission ray in between transmitter and receiver when applying this model. One reasonable criterion to determinate if this model can be applied is given by [10]:

$$\Delta\phi_{[rad]} \approx \frac{2\pi}{\lambda_{[m]}} \frac{h_{GS[m]}\ h_{A[m]}}{h_{GS[m]} + h_{A[m]}} \frac{d_{[m]}}{R_{e[m]}} < 1 \quad (2.2)$$

where:

- $\Delta\phi$: Phase difference between using the Flat Earth and Spherical Earth Models;
- λ: Wavelength of the transmitted signal;

- h_{GS}: Height of ground station;
- h_A: Height of aircraft.
- R_e : effective Earth's radius;

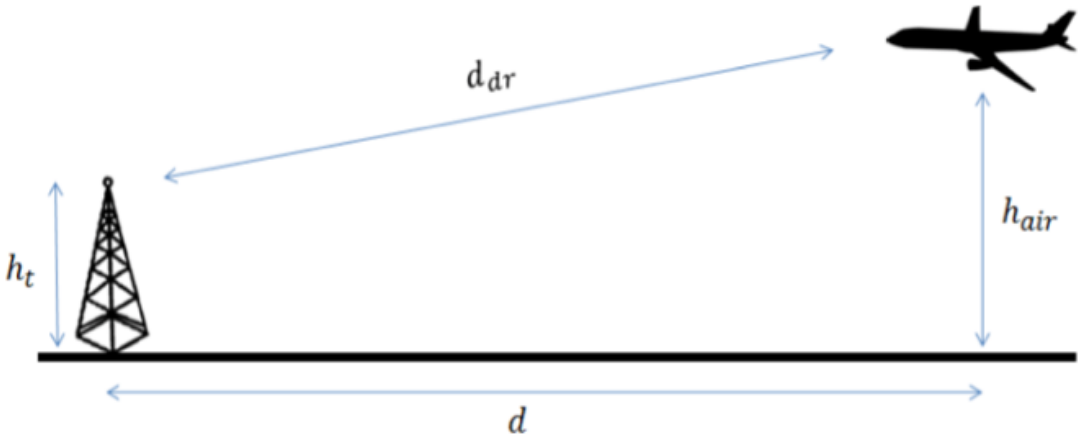

Figure 2-2: Diagram of Flat Earth Model (extracted from [33]).

However, for some cases, the direct ray can be obstructed by an obstacle that may cause extra attenuation. Therefore, an analysis should be done by verifying if the first Fresnel's Ellipsoid is obstructed, since most of the transmitted energy is concentrated in that region. Equation (2.3) provides the radius of Fresnel's Ellipsoid of order n depending on the distance x to the terminals. The ellipsoid is symmetric so the distance x can be relative to any of the antennas [14].

$$R_{f\,e,n[m]} = \sqrt{n\frac{x_m(d_{dr[m]} - x_{[m]})}{d_{dr[m]}}\lambda_{[m]}} \tag{2.3}$$

where:

- $R_{f\,e,n}$: radius of the Fresnel Ellipsoid of order n in a point with a distance x to the terminal;
- n: order of the Fresnel Ellipsoid;
- x: distance from the point to the terminal.

If the first Fresnel's Ellipsoid is obstructed, the attenuation from the obstacle is considerable. In order for the Knife-Edge model to work, the dimension of the obstacle needs to be larger than the wavelength of the signal [10]. Since the frequencies in this work are in the VHF band, they comprise a wavelength of roughly 3 m, thus fulfilling the conditions of this model. The higher the obstruction in the first Fresnel's Ellipsoid is, the higher is the attenuation and subsequent bigger will be the parameter ν defined as [10]

$$\nu = h_{ofe[m]}\sqrt{\frac{2d_{[m]}}{\lambda_{[m]}d_{t[m]}d_{r[m]}}} \tag{2.4}$$

where:

- ν: obstacle impediment coefficient;
- h_{ofe}: height from the tip of obstacle to the centre of the ellipsoid (it can have negative values when the obstacle is below the line of sight);

- d_t: distance from the obstacle to the transmitter;
- d_r: distance from the obstacle to the receiver.

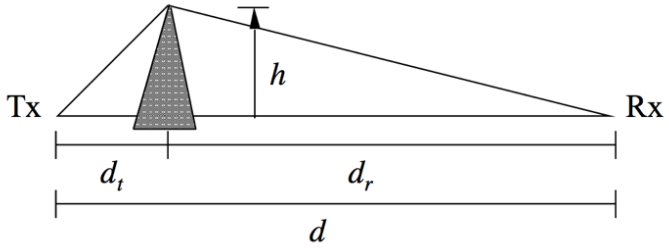

Figure 2-3: Knife-edge model geometry (extracted from [10]).

The Knife-Edge model path loss generated by the obstacle can be approximated by (2.5). For values of $\nu \leq -0.8$ the path loss is considered negligible [10].

$$L_{KE[dB]} = 6.4 + 20\log(\nu + \sqrt{\nu^2 + 1}) \tag{2.5}$$

The Deygout method presents a reasonable approach for situations where there are multiple obstacles, [33]. First, the ν coefficient is calculated for all obstacles, and the one with the highest value of ν is labelled as the main obstacle. One obtains the path loss caused by the main obstacle using (2.5), and then the path is divided in two segments with the main obstacle's edge as a new terminal point. Next, the two smaller paths are analysed and the same process is repeated until all obstacles are considered. The total path loss caused by the obstacles corresponds to the sum of all path losses. Note that other more realistic models to estimate the extra attenuation from the obstacles could be use in order to estimate better approximations of the true value like the diffraction by a cylindrical obstacle model.

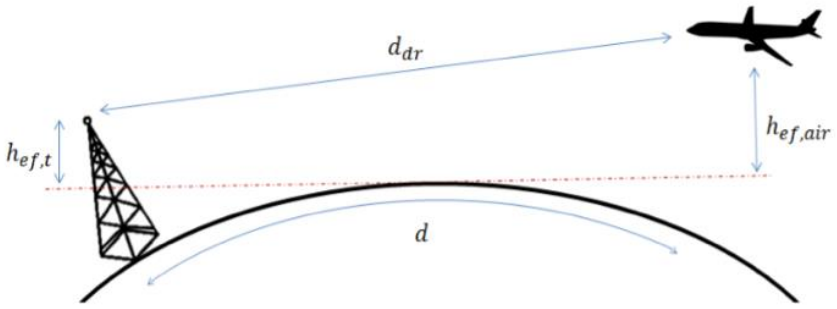

Figure 2-4: The Spherical Earth Model and the Flath Earth equivalent parameters (extracted from [33]).

In cases where the aircraft is far from the controller, i.e. when (2.2) is not valid, the Spherical Earth Model needs to be considered. In this case, instead of the physical height of the stations, one uses the effective heights of the antennas expressed by [33],

$$h_{ef,GS[km]} = h_{t[\mathrm{km}]} - \frac{d_{GS}^2}{2R_{[\mathrm{km}]}} \tag{2.6}$$

$$h_{ef,A[km]} = h_{air[\mathrm{km}]} - \frac{d_A^2}{2R_{[\mathrm{km}]}} \quad (2.7)$$

where:

- d_{GS}: ground distance between the station and the reflection point;
- d_A: ground distance between the aircraft and the reflection point;
- $h_{ef,GS}$: equivalent effective height of the terminal in the Flat Earth model;
- $h_{ef,A}$: equivalent effective height of the aircraft in the Flat Earth model;
- R: Earth's radius.

In cases where the line-of-sight is obstructed, it is also needed to determinate the path loss generated by the obstacles. Also for long distance communications, the curvature of the Earth can interfere with the line-of-sight, therefore the radius of the Earth's surface should be considered [33].

$$R_e = kR_{[\mathrm{km}]} \quad (2.8)$$

where:

- R_e : effective Earth's radius;
- k: multiplication factor, typically 4/3.

In addition, the distance to the radio horizon should also be calculated by [33]

$$d_{RH[\mathrm{km}]} = \sqrt{\left(R_{e[\mathrm{km}]} + h_{t,MSL[\mathrm{km}]}\right)^2 - R_{e[\mathrm{km}]}^2} \approx \sqrt{2R_{e[\mathrm{km}]}h_{t,MSL[\mathrm{km}]}} \quad \text{, for } R_e \gg h_{t,MSL} \quad (2.9)$$

where approximation it is done for $R_e \gg h_{t,MSL}$ and

- d_{RH}: distance from the terminal to its radio horizon;
- $h_{t,MSL}$: height above Mean Sea Level (MSL) of the terminal.

Therefore, the maximum propagation distance of the radio link between the aircraft and the ground station is:

$$d_{LOS[\mathrm{km}]} = \sqrt{2R_{e[\mathrm{km}]}h_{A,MSL[\mathrm{km}]}} + \sqrt{2R_{e[\mathrm{km}]}h_{GS,MSL[\mathrm{km}]}} \quad (2.10)$$

where:

- $h_{A,MSL}$: Aircraft height above mean sea level;
- $h_{GS,MSL}$: Ground station height above mean sea level.

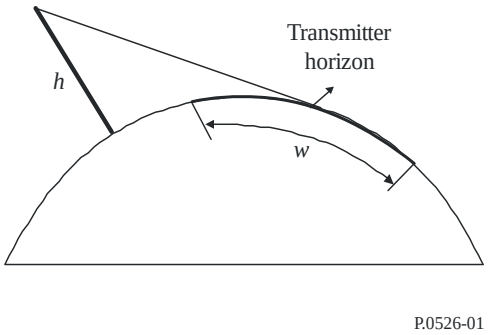

Figure 2-5: Definition of penumbra width (extracted from [26]).

However, a transition from light to shadow defines the penumbra region that takes place along a narrow strip (penumbra width) in the boundary of geometric shadow. Figure 2-5 shows the penumbra width (w) in the case of a transmitter located a height, h, above a smooth spherical earth, which is given by:

$$w = \left[\frac{\lambda R_e^2}{\pi}\right]^{\frac{1}{3}} \tag{2.11}$$

One way to extend the distance over the horizon is to use higher antennas. However, in that case, a higher power input will be needed for the signal to travel that farther.

The only mechanisms for radio propagation beyond the horizon that occur permanently for frequencies larger than 30 MHz are those of diffraction over the Earth's surface and scatter from atmospheric irregularities. Attenuation from diffracted signals increases very rapidly with distance and frequency, and eventually the principal mechanism is that of tropospheric scatter. Both mechanisms may be used to establish "trans-horizon" radio communication. Because of the dissimilarity of the two mechanisms, it is necessary to consider diffraction and tropospheric scatter paths separately for the purposes of predicting transmission loss.

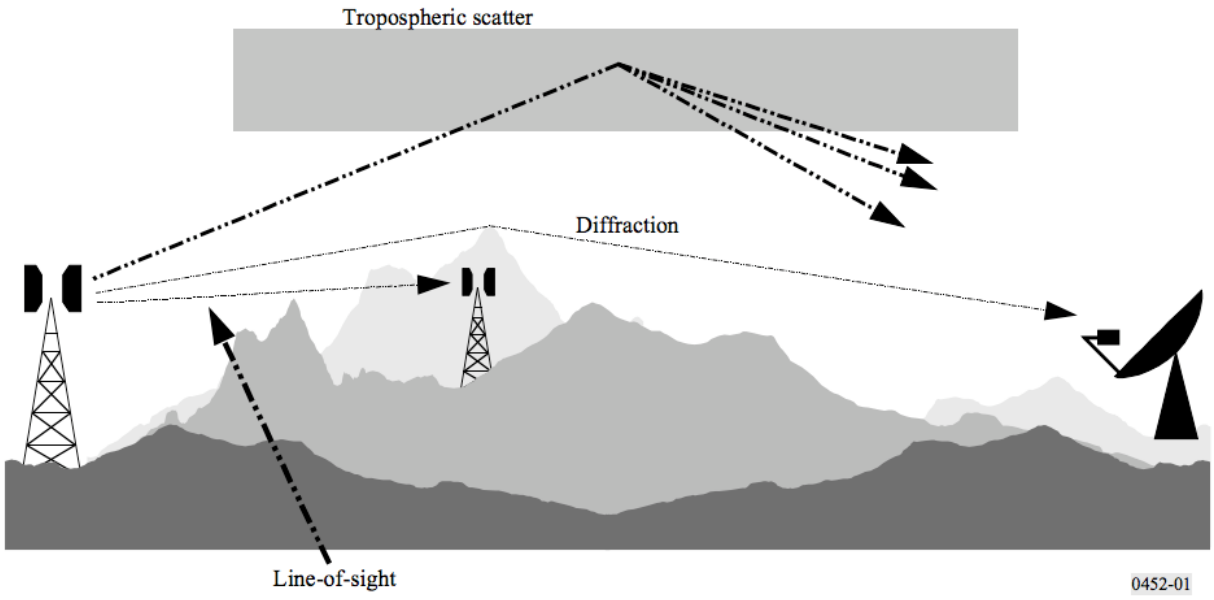

Figure 2-6: Propagation mechanisms: Line-of-sight, Diffraction and Troposcatter (extracted from [26]).

The additional transmission loss due to diffraction over a spherical Earth can be computed by the classical residue series formula. In [26], there is a numerical calculation method that only works for trans horizon paths, though the results are more reliable in the deep shadow area well beyond the horizon.

The diffraction field strength, *E*, relative to the free-space field strength, E_O, is given by [26]:

$$20\log_{10}\frac{E}{E_O} = F(X) + G(Y_1) + G(Y_2) \text{ [dB]} \tag{2.12}$$

where X is the normalized length of the path between the antennas at normalized heights Y_1 and Y_2 (and where $20\log_{10}\frac{E}{E_O}$ is generally negative).

Therefore, the total path loss for a distance d due to diffraction by Earth's diffraction can be determined by:

$$L_{dif\,[\mathrm{dB}]} = -[F(X) + G(Y_1) + G(Y_2)] + L_{fs[\mathrm{dB}]} \tag{2.13}$$

In practical units [26]:

$$X = 2.2 \times \beta \times f_{[\mathrm{MHz}]}^{1/3} \times R_{e[\mathrm{km}]}^{-2/3} \times d_{[\mathrm{km}]} \tag{2.14}$$

$$Y = 9.6 \times 10^{-3} \times \beta \times f_{[\mathrm{MHz}]}^{2/3} \times R_{e[\mathrm{km}]}^{-1/3} \times h_{[\mathrm{m}]} \tag{2.15}$$

where:

- h: antenna's height above the spherical Earth.

β is a parameter allowing for the type of ground and for polarization. It is related to K (normalized factor for surface admittance) by the following semi-empirical formula [26]:

$$\beta = \frac{1 + 1.6K^2 + 0.75K^4}{1 + 4.5K^2 + 1.35K^4} \tag{2.16}$$

As stated in [26], for vertical polarization below 20 MHz over land or 300 MHz over sea, β must be calculated as a function of K.

$$K^2 \approx 6.89\frac{\sigma_{[\mathrm{S/m}]}}{k^{2/3} f_{[\mathrm{MHz}]}^{5/3}} \tag{2.17}$$

where:

- σ: electrical conductivity ($\sigma = 5\ \mathrm{S/m}$ for the sea water).

The distance term is given by [26]:

$$F(X) = 11 + 10\,log_{10}\,X - 17.6X \tag{2.18}$$

The height gain term, *G*(*Y*) is given by [26]:

$$G(Y) \cong 17.6(Y - 1.1)^{\frac{1}{2}} - 5\log_{10}(Y - 1.1) - 8 \qquad \text{for } Y > 2 \tag{2.19}$$

$$G(Y) \cong 20\log_{10}(Y + 0.1Y^3) \qquad \text{for } 10K < Y < 2 \tag{2.20}$$

$$G(Y) \cong 2 + 20\log_{10} K + 9\log_{10}\frac{Y}{K}\left[\log\left(\frac{Y}{K}\right) + 1\right] \qquad \text{for } \frac{K}{10} < Y < 10K \tag{2.21}$$

$$G(Y) \cong 2 + 20\log_{10} K \qquad \text{for } Y < \frac{K}{10} \tag{2.22}$$

The mechanism of troposcatter is shown in Figure 2-7. The antennas of the two stations cannot "see" each other, yet they can each "see" a common volume of the atmosphere. Because of the atmospheric inhomogeneities, signals from one station are going to be transmitted and some part of the energy is scattered back towards the Earth, allowing the receiver station to pick up the signal.

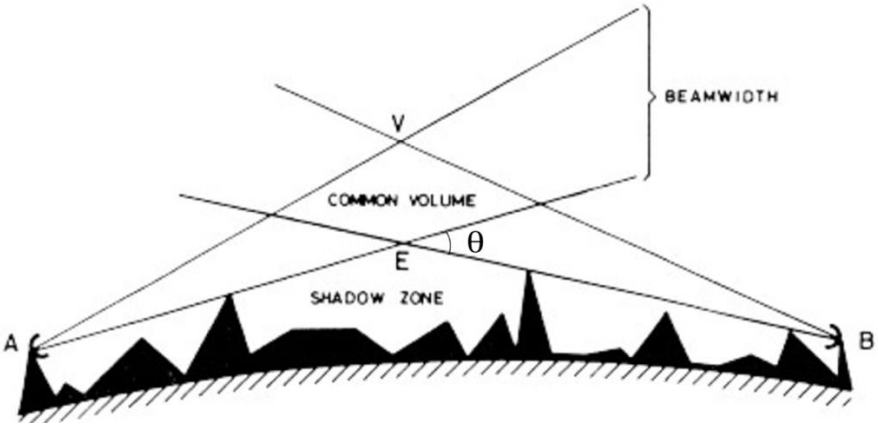

Figure 2-7: Profile of a typical troposcatter path (extracted from [15]).

As stated in [17], signals received by means of tropospheric scatter show both slow and rapid variations. Slow variations are due to overall changes in refractive conditions in the atmosphere and the rapid fading to the motion of small-scale irregularities. Slow variations are well described by distributions of the hourly-median transmission loss, which are approximately log-normal with standard deviations between about 4 and 8 dB, depending on climate. The rapid variations over periods up to about 5 min are approximately Rayleigh distributed.

In determining the performance of trans-horizon links for geometries in which the tropospheric scatter mechanism is predominant, it is normal to estimate the distribution of hourly-median transmission loss for non-exceedance percentages of the time above 50%. A simple semi-analytical technique for predicting the distribution of average annual transmission loss in this range is given in [17].

The following step-by-step procedure is recommended for estimating the average annual median transmission loss $L(q)$ not exceeded for percentages of the time q greater than 50%. The procedure requires the link parameters of great-circle path length d (km), frequency f (MHz), transmitting antenna gain G_t (dB), receiving antenna gain G_r (dB), horizon angle θ_t (mrad) at the transmitter, and horizon angle θ_r (mrad) at the receiver.

$$L(q)_{[\mathrm{dB}]} = M + 30\log_{10} f_{[\mathrm{MHz}]} + 10\log_{10} d_{[\mathrm{km}]} + 30\log_{10}\theta_{[\mathrm{mrad}]} + L_{N[\mathrm{dB}]} + L_{C[\mathrm{dB}]} - G_{t[\mathrm{dBi}]} - G_{r[\mathrm{dBi}]} - Y(q)_{[\mathrm{dB}]} \tag{2.23}$$

The determination of the appropriate climate for the common volume of the link is based on Fig.1 of [17]. Therefore, it is possible to observe that Azores Archipelago is in the climate zone number 4, so by Table 2 of [17]:

- $M = 38.5\,\mathrm{dB}$ (meteorological parameter);
- $\gamma = 0.27/\mathrm{km}$ (atmospheric structure parameter).

The scatter angle shown in Figure 2-7 as θ is obtained by [17]:

$$\theta_{[\mathrm{mrad}]} = \theta_{e[\mathrm{mrad}]} + \theta_{t[\mathrm{mrad}]} + \theta_{r[\mathrm{mrad}]} \tag{2.24}$$

$$\theta_{e[\mathrm{mrad}]} = d_{[\mathrm{km}]} \times \frac{10^3}{R_{e[\mathrm{km}]}} \tag{2.25}$$

The transmission loss dependence L_N n the height of the common volume estimation is:

$$L_{N[\mathrm{dB}]} = 20\log_{10}(5 + \gamma H) + 4.34\gamma h \tag{2.26}$$

$$H_{[\mathrm{km}]} = \frac{\theta d}{4 \times 10^3} \tag{2.27}$$

$$h_{[km]} = \frac{\theta^2 R_{e[km]}}{8 \times 10^6} \tag{2.28}$$

Estimation of the aperture-to-medium coupling loss L_C:

$$L_{C[\mathrm{dB}]} = 0.07e^{0.055(G_r + G_t)} \tag{2.29}$$

Finally, the conversion factor $Y(q)$ for non-exceedance percentages q other than 50% is:

$$Y(q)_{[\mathrm{dB}]} = C(q)Y(90)_{[\mathrm{dB}]} \tag{2.30}$$

where $Y(90)$ is the conversion factor for $q = 90\%$, and for the climate number 4, one has:

$$Y_{90} = -11.5 \qquad \text{for } d_S < 100 \tag{2.31}$$

$$Y_{90} = -8.519 \times 10^{-8} d_s^3 + 7.444 \times 10^{-5} d_S^2 - 4.18 \times 10^{-4} d_S - 12.1 \qquad \text{for } 100 < d_S < 550 \tag{2.32}$$

$$Y_{90} = -4 \qquad \text{otherwise} \tag{2.33}$$

where

$$d_{S[\mathrm{km}]} = \frac{\theta \times R_E}{1000} \tag{2.34}$$

Also, contributing for the extension of the communication range are the ducts and the layer reflection/refraction however they occur for smaller percentages of time, and for that reason they are referred as short-term propagation/interference mechanisms.

In the presence of a ducting layer, the concept of horizon no longer has any precise meaning, and very distant points may be in LOS. Radio rays can get trapped in a duct if the transmitting antenna is within a duct and elevation angles are low. If refractivity conditions are normal with a fixed refractivity gradient, the critical elevation angle γ for captured rays is [16]:

$$\gamma = \sqrt{2 \times 10^{-6} \Delta h \left|\frac{dM}{dh}\right|} \text{ radians} \quad (2.35)$$

where:

- $\frac{dM}{dh}$: vertical gradient of modified refractivity;
- Δh: height of top of duct above transmitting antenna.

Ducting, the trapping of signals in waveguide-like duct formed by atmospheric layers of different refractive index, can propagate VHF signals with very little loss over long distances. Unfortunately, ducting is rare and relatively unpredictable, and it is difficult to calculate the magnitude, length, and frequency characteristic of a duct in advance. The effects on VHF transmission depend mainly on the location of the receiving antenna. If the receiving antenna is within the duct, stronger signal will be received and transmission beyond the horizon is made possible. There are three different types of ducts in communications over sea: Evaporation, Surface-based and Elevated.

Evaporative ducts form over water, where the cooling near the surface from evaporation results in cool air below warm air and a temperature inversion. The thickness of the evaporation duct in the North Sea typically extends to 5 m above the sea. Nevertheless, according to [17], only for frequencies above 2 GHz the evaporation ducting thus for VHF propagations are not that relevant.

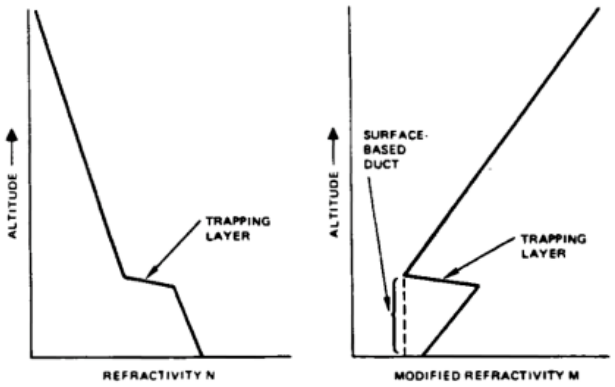

Figure 2-8: Refractivity profiles showing surface-based duct (extracted from [18]).

In cases where the continental influence due to the advection of warm and dry air over the cooler sea surface appear in oceanic regions, surface ducts (Figure 2-8) take over evaporation ducts as dominant propagation. According to [13], that happens in the North Sea area about 1.7 % of the time and contrary to evaporation ducts surface-based ducts can support frequencies as low as 100 MHz.

Elevated ducts are like surface-based ducts. They can also support long-range communications for frequencies above 100 MHz and are created by elevated trapping layer with mean base height of 1.2 km from surface [19]. However, it is not guaranteed that getting trapped in a duct will lead to a successful long-range communication without losing a lot of strength in the signal.

2.3 Antennas for Aeronautical Communications

This section contains information about some antennas used for aeronautical purposes and is based in [6], [21] and [20].

2.3.1 Omnidirectional Antennas

The radiation pattern of a vertical dipole is omnidirectional when in free space radiating the same amount of power in any radiation power in all positions perpendicular to the antenna, with the signal strength dropping to zero on the antenna axis. The relative gain of a linear dipole is given by [22]:

$$F(\theta) = \frac{\left(\cos\left(\frac{\pi L_{[\mathrm{m}]}}{\lambda_{[\mathrm{m}]}}\right)\cos\theta\right) - \left(\cos\left(\frac{\pi L_{[\mathrm{m}]}}{\lambda_{[\mathrm{m}]}}\right)\right)}{\sin\theta} \tag{2.36}$$

where:

- L: length of the dipole;
- θ: angle between the vertical plane and the beam direction.

A half-wave dipole has a maximum gain of 2.15 dBi, in the plane perpendicular to the antenna axis. Adding wire connecting the two ends on a half-wave dipole, can give a fourfold increase in feed impedance, turning it less prone to impedance variations. As for the radiation pattern and gain, they are very similar to the latter.

Other type of antennas that are used in aeronautical purposes are the quarter-wave vertical antenna and 5/8λ vertical antennas. A quarter-wave vertical antenna consists of a quarter wave above a ground plane antenna. One thing that is very important when installing VHF stations is the height, since antennas need to be raised enough to be above nearby obstructions. Also, it is omnidirectional in the horizontal plane and consists of a single end-fed element. Most of the energy is concentrated on the horizontal lobe where it is considered an equal gain in all directions. A 5/8λ vertical antenna is used when an omnidirectional high gain antenna is needed. Nevertheless, the gain continues to be greater in the horizontal orientation. Relative to a dipole, the peak gain is close to 4dBd.

However, sometimes the gain of only one antenna is not enough and for that reason it is needed to increase the number of antennas, thus arrays of dipoles or folded dipoles are often used as ground station antennas. A collinear antenna array is a set of dipoles mounted parallel and collinear to each other and they radiate vertically polarized radio waves. Stacking multiple dipoles in a vertical collinear array, increases the radiation power in horizontal directions and, for ground-to-air communications, reduce the power radiated down toward the earth where is wasted. Doubling dipoles would mean theoretically doubling the gain (3 dB) however, that does not happen due to spread radiation imperfections and losses. A collinear is suited for long distance communications in a central position and it is ideal for mounting at the top of a structure or of a tower or pole. The radiation pattern of an array is given by [25]:

$$G_{array}(\theta,\phi) = G_{antenna} \times F_{aa}(\theta,\phi) \quad (2.37)$$

where:

- $G_{antenna}$: gain of the array antenna element;
- F_{aa}: Antenna array factor.

This is only valid because the distance between elements is considerable. F_{aa} depends on the excitation distributed among the various antennas and the distance between elements and is given by [25]:

$$F_{aa}(\theta,\phi) = \sum_{n=1}^{N_{ant}} e^{j(n-1)\gamma_{del}} = e^{\frac{j(N_{ant}-1)\gamma}{2}} \times \frac{\sin\left(\frac{N_{ant}\gamma_{del}}{2}\right)}{\sin\left(\frac{\gamma_{del}}{2}\right)} \quad (2.38)$$

$$\gamma_{del}(\theta,\phi) = k d_{ant[\mathrm{m}]} \cos\theta + \delta_{[\mathrm{rad}]} \quad (2.39)$$

where:

- N_{ant}: number of elements in the array;
- γ_{del}: phase delay;
- k: wave number;
- d_{ant}: distance between the dipoles;
- δ: electric phase difference between the N^{th} antenna and the reference one.

Thought, in cases where the traffic is more concentrated in one section than the others, directional antennas can be more useful than omnidirectional ones. The Yagi antenna is a higher directive antenna because of its design, which consists of a reflector, a driven element and directors. Starting firstly by the driven element, which is normally a half wavelength dipole or a folded dipole, it is the Yagi's element that is fed with power. Behind the driven element, there is a reflector that will improve the performance of the antenna, by reducing the level of radiation or pick-up from behind the antenna (backwards direction) and, because of that, adding typically 4 or 5 dB of gain in the forward direction. More gain will come from the directors, which are placed in front of the driven element, in the direction of the maximum radiation. Each director adds around 1 dB of gain in the forward direction, thus as the number of directors increases that gain per director is reduced. Also, for high gain levels, the antenna becomes very long and the gain is limited to around 20 dBi.

The panel antenna consists of a single simple half-wavelength dipole mounted at a pre-determined distance from an integral reflecting plane, or for more complicated arrays of 4 (or more) narrow or broad-band, linearly or circularly polarized elementary radiators.

2.4 State of the Art

In [26], it is stated that the belief that VHF services could be used to provide reliable communications beyond the horizon started in 1960, in an extended range VHF symposium hosted by International Aerodio Ltd. After that, many installations have been put in operation worldwide. However, only recently, and because of the increase of traffic in oceanic airspace, VHF extending communication systems became a clear choice. As said before, there are a few ways in which this happens, such as tropospheric scattering, atmospheric refraction and diffraction. Whatever the means, the signal is likely to be significantly attenuated. So, all over-the-horizon coverage systems involve the boosting of transmitted power and the reception of weak signals. This requires the use of some or all the following:

- High Power Amplifiers on Transmitters.
- Low-Noise Pre-Amplifiers on Receivers.
- High Gain - and consequently directional - Antennas.

Clearly such systems can exacerbate the difficulties associated with interference between radios, so this must all be carefully considered in the system design.

According to [23], a Northrop Grumman subsidiary, Park Air Systems has already implemented some 20 over-the-horizon VHF systems around the world, including in Greenland, Iceland, Singapore and China. Over-the-horizon VHF communications systems are preconfigured and transportable. They are built and tested at Park Air's facility in Peterborough, UK, before being sent for installation and commissioning.

The one implemented in China exceeded the expectations and its location is at the southern coastal city of Sanya, providing long-range air traffic communication over the South China Sea, and it was an agreement between the aviation administration of China and neighbouring Vietnam to establish a joint area of responsibility (AOR) over the South China Sea. Typically, air traffic using southern routes is transiting from Bangkok, Kuala Lumpur and Singapore to destinations such as Hong Kong and Japan.

With the Park Air's solution, there is no need to change the airborne radios meeting ICAO standards and uses a ground transmitter of 250 W carrier power to achieve the desired field strength for aircraft at long range.

At the Sanya's installation, the transmitter is connected to a pair of directional antennas aligned to project a powerful beam in the required direction. Each antenna is composed by a six elements' stacked Yagi array with four dipoles radiators mounted on a horizontal support per element, mounted on a tower/platform with power level of some 750 W. The resulting horizontal beam width is some 90º, and the vertical beam width is approximately 60º. This beam is broad enough to provide coverage for all aircraft flying within the area of responsibility, but it is concentrated enough to afford sufficient forward gain to reach aircraft out to the maximum range and altitude.

Another case where the VHF was extended was in Dutch Caribbean Air Navigation Service Provider (DC-ANSP) to deliver ground-to-air communication system for deployment in Curacao. Curacao is one of the busiest airports in the Caribbean region with high flight traffic between North and South America.

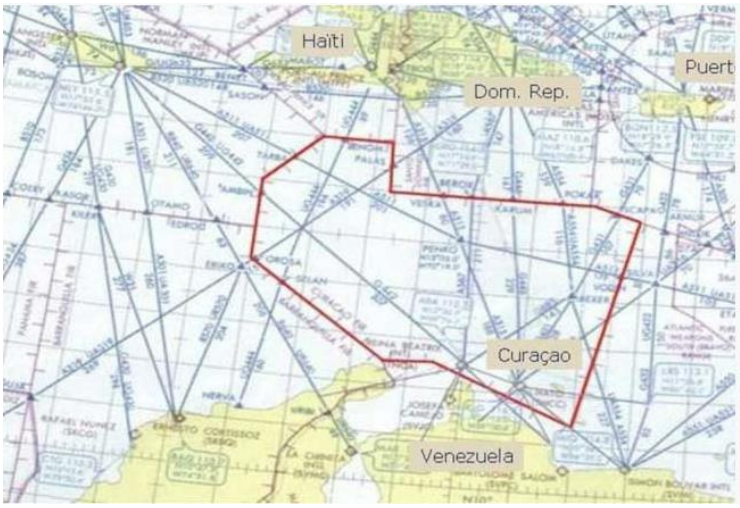

Figure 2-9: Curacao Flight Information Region.

As said in [27], Northrop Grumman Park Air Systems initially conducted a site survey, followed by a detailed assessment of the predicted coverage that would be achieved. The latest high power 200 W T6 VHF radios have been delivered as part of the system. The installation of the radios, to be located on the hilltop site Seru Gracia on the island of Curacao (Figure 2-9), will provide ground-to-air communications for pilots throughout the Curacao Flight Information Region, one of the busiest in the Caribbean region due to the high volume of flights between North and South America. The set of extended range communication solutions includes transmitters with a power of up to 300 W, mast-head amplifiers and high-gain antenna arrays.

Other successful example of VHF coverage extension is shown in the ICAO's report [28], i.e., the enhancement of VHF coverage over Indian airspace in the Oceanic region. The Air control centre coverage of Mumbai and Trivandrum airport over Arabian Sea has been enhanced by putting Remote Controlled Air to Ground Communication (RCAG) at Agatti (an island in Arabian Sea) controlled from Mumbai and Trivandrum airport. To ensure further improvement, Airports Authority of India (AAI) deployed high power VHF Transmitter with directional antenna at Chennai and Port Blair and High power VHF Transmitters at Kolkata and Vishakhapatnam.

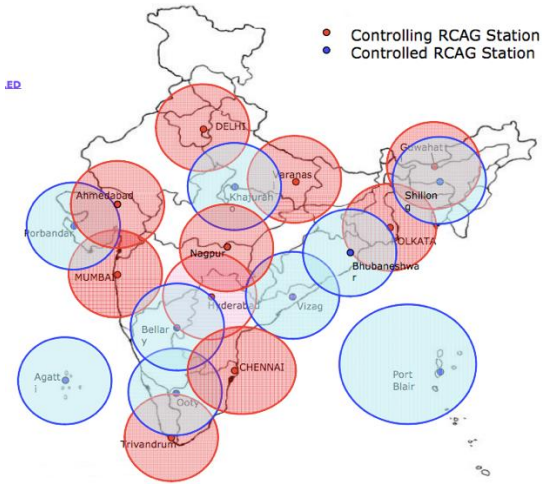

Figure 2-10: RCAG stations in India (extracted from [29]).

Figure 2-10 presents the RCAG stations in India. Special attention to the Chennai and Port Blair RCAG stations, with directive antennas and larger coverage when comparing with all the others, in order to improve the coverage in the Bay of Bengal.

Chapter 3

Models and simulator description

This chapter concerns the proposal, description, implementation, and assessment of the model in order to observe the extension of coverage theoretically in Azores' with reliable results.

3.1 Model Development

The purpose of this section is to describe the theoretical models employed in solving the research problem of this dissertation.

3.1.1 Model Overview

Oceanic Azores' FIR is an incredibly vast area of 5 138 160.886 km^2, and it covers a wide area of the North Atlantic. The purpose of this thesis is to extend communication aeronautical services coverage over the ocean via antenna optimization. Figure 3-1 presents the outline of the proposed model with the constraints, specifications and steps required to estimate the operational system coverage for voice communication between the pilot and the controller.

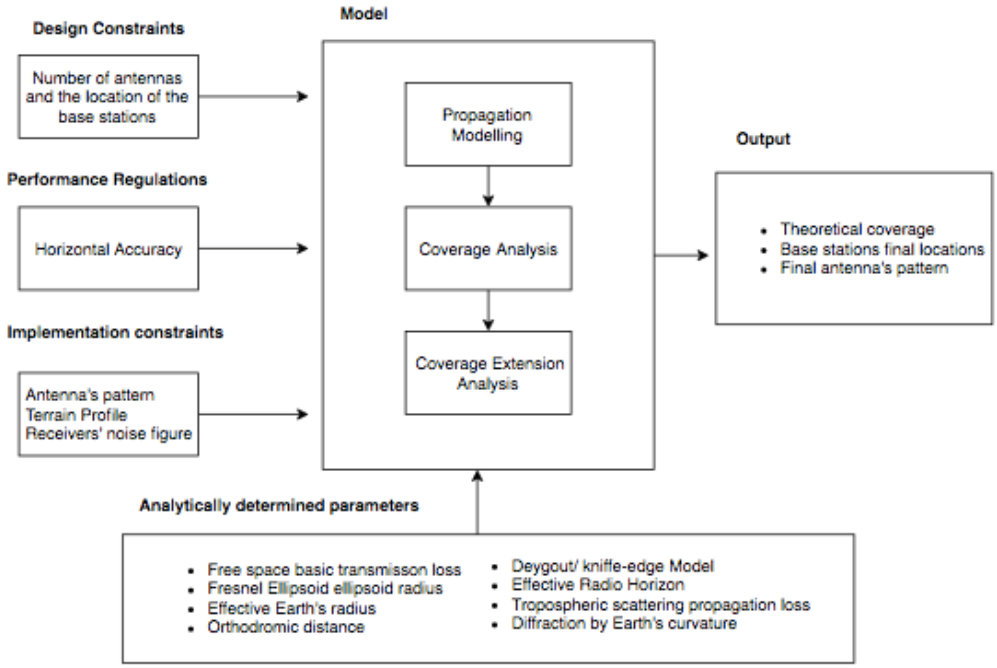

Figure 3-1: Model Overview.

In the interest of studying the coverage for that vast area, ground stations are set fixed into their possible locations with their well-known radiation patterns, noise figures, sensitivities and height. On the other hand, the coordinates of the aircrafts change from point to point among a defined geographic volume, i.e., the develop model assumes the aircraft as a point target in a horizontal plane parallel to the Earth leaving out of account the yaw, pitch and roll angles.

Regarding the coverage analysis, it can be divided into two situations: line-of-sight propagation coverage analysis and over-the-horizon ones. The chosen mechanism is the one with lower path loss.

It is worth stating that LOS coverage analysis should consider the terrain profile and the first order Fresnel ellipsoid model to determine if an aircraft and a GS are in view, or if their radio-path is blocked

by the terrain and that the terrain profile is referenced to the 1984 World Geodetic System (WGS84) with heights referenced to the 1996 Earth Gravitational Model (EGM96) geoid [30].

After the determination of the total path loss, one must do the sensitivity coverage analysis to determinate if the signal at the receiver is above the minimum received power threshold (sensitivity of the receiver) required for a proper voice communication. The current ground stations are not enough to cover all the FIR's area; therefore, some changes must be done. The solution can come by changing the radiation patterns of the transmitting antennas and/or changing their location or, in the last case, adding new ground stations.

3.1.2 Propagation Models

Recommended field strengths for extended-range VHF communications are defined within ICAO Annex 10, [26], for both the aircraft and the ground installation. Since the aircraft is more compact and has a lower gain antenna compared with the ground station antenna, the electric field strength must be significantly higher, something that can suffer performance impairment due to airframe shielding, aircraft-generated electrical noise, and other system factors. In [26], it is stated that the sensitivity of the aircraft's receiving function should be such as to provide on a high percentage of occasions an audio output signal with a wanted/unwanted ratio of 15 dB for the output voice signal, with a 50% amplitude modulated (A3E) radio signal having a field strength of 30 μV/m (when planning extended ranges), while for the ground station the field strength must be no less than 20 μV/m.

It is also worth noting that, at VHF and UHF bands, seawater refraction index is about (-1) and therefore the sea surface is a good reflector for these radio waves. In some conditions, detected signals in the receiver are summation of direct and reflected.

The received power can be now obtained by [10]:

$$P_{r[\mathrm{dBm}]} = -77.21 + E_{r[\mathrm{dB\mu V/m}]} + G_{r[\mathrm{dBi}]} - 20\log f_{[\mathrm{MHz}]} \tag{3.1}$$

where:

- E_r: Electric Field Strength in the receiving antenna.

The received power can also be expressed by [10]:

$$P_{r[\mathrm{dBm}]} = P_{EIRP[\mathrm{dBm}]} + G_{r[\mathrm{dBi}]} - L_{p[\mathrm{dB}]} = P_{t[\mathrm{dBm}]} + G_{t[\mathrm{dBi}]} + G_{r[\mathrm{dBi}]} - L_{p[\mathrm{dB}]} \tag{3.2}$$

where:

- P_{EIRP}: Equivalent isotropic radiated power;
- P_t: Power fed to the transmitting antenna;
- L_p: Total path loss between the transmitting and the receiving antennas.

Because of the power sensitivity of both airborne and ground station antennas, and due to the significantly decrease of the signal strength beyond the horizon, the only possible way to improve the received power is by increasing the gain of the ground station antenna or the transmitting power of the

ground station antenna since both the transmitting power and the gain of the aircraft cannot be changed and the frequency is limited to the air band. However, most of the time it is useless to increase the transmitting power of the GS, because even though the signal is strong enough for the controller to communicate with the pilot, the pilot may not be capable of communicating with the controller. Vice-versa can also happen, when the aircraft is close to the antenna.

For this thesis, the three mechanisms - line-of-sight propagation, diffraction by Earth's curvature and troposcatter propagation – are analysed individually and the determination of their path loss comes from (2.1), (2.13) and (2.22) respectively.

For the communication to happen correctly, the net link margin must be above a defined value. The net link margin provides a measure of the power surplus in the link, between the operating point and the point where the link can no longer be maintained:

$$\Delta P_{r[\mathrm{dB}]} = P_{r[\mathrm{dBm}]} - P_{r,min[\mathrm{dBm}]} \tag{3.3}$$

$$P_{r,min[\mathrm{dBm}]} = -77.21 + E_{r,min[\mathrm{dB\mu V/m}]} + G_{r,min[\mathrm{dBi}]} - 20\log f_{[\mathrm{MHz}]} \tag{3.4}$$

where:

- ΔP_r: Received Power above the threshold/sensitivity;
- $P_{r,min}$: Sensitivity/Threshold - Lowest power level at which the receiver can detect an RF signal;
- $E_{r,min}$: Lowest field strength such as to provide on a high percentage of occasions an audio output signal with a wanted/unwanted ratio of 15 dB, with a 50 per cent amplitude modulated (A3E) radio signal. ICAO recommends these values to be [31]:
    - Airborne: $E_{r,\mathrm{min}} \approx$ 29.54 dBµV/m;
    - Ground Station: $E_{r,\mathrm{min}} \approx$ 26.06 dBµV/m;
- $G_{r,min}$: Receiver's lowest gain power.

As stated in [30], the law of cosines for planar triangles and the Spherical Earth Model can be used to produce estimators for the propagation path length, and for the elevation angles at the antennas. The Spherical Earth Model is not without error, approximating the Earth by a sphere introduces an error proportional to the Earth's flattening, bellow 1%; this approximation is reasonable for ΔP_r estimation. For succinctness in the presentation of the models, one starts by defining the following quantities,

$$r_{A[\mathrm{km}]} = R_{E[\mathrm{km}]} + h_{A,MSL[\mathrm{km}]} \tag{3.5}$$

$$r_{GS[\mathrm{km}]} = R_{E[\mathrm{km}]} + h_{GS,MSL[\mathrm{km}]} \tag{3.6}$$

$$\Delta h^{A}_{GS[\mathrm{km}]} = h_{A,MSL[\mathrm{km}]} - h_{GS,MSL[\mathrm{km}]} \tag{3.7}$$

where:

- r_A: effective distance of the aircraft's antenna to the Earth's centre;
- r_{GS}: effective distance of the ground station's antenna to the Earth's centre;
- Δh^{A}_{GS}: difference between aircraft and Ground stations height;
- R_E: effective Earth radius;

- $h_{A,MSL}$: Aircraft height above mean sea level;
- $h_{GS,MSL}$: Ground station height above mean sea level.

Concerning the radio-path length, it is, firstly, required to estimate the geocentric angle that is defined as the angle formed by the imaginary straight line that joins two given points with the Earth's centre [30],

$$\theta_{c[\mathrm{rad}]} = \arccos(\cos(\phi_{A[\mathrm{rad}]})\cos(\phi_{GS[\mathrm{rad}]})\cos(\lambda_{A[\mathrm{rad}]} - \lambda_{GS[\mathrm{rad}]}) + \sin(\phi_{A[\mathrm{rad}]})\ \sin(\phi_{GS[\mathrm{rad}]})) \quad (3.8)$$

where:

- θ_c: geocentric angle between the Ground station and the aircraft.

Therefore, by knowing the altitudes and the geocentric angle between the aircraft and the base, it is now possible to estimate the radio-path length [30],

$$d_{[\mathrm{km}]} = 2 \times R_{e[\mathrm{km}]} \sin\frac{\theta_{c[\mathrm{rad}]}}{2} \sqrt{\left(1 + \frac{h_{GS,MSL[\mathrm{km}]}}{R_{e[\mathrm{km}]}}\right)\left(1 + \frac{h_{A,MSL[\mathrm{km}]}}{R_{e[\mathrm{km}]}}\right) + \left(\frac{\Delta h^{A}_{GS[\mathrm{km}]}}{2R_{e[\mathrm{km}]} \sin\frac{\theta_{c[\mathrm{rad}]}}{2}}\right)^2} \quad (3.9)$$

where:

- d: radio-path length.

The authors in [30] state that this model is numerically better-conditioned than the analytically equivalent obtained by direct application of the law of cosines for planar triangles to the triangle formed by the Earth's centre, the ground station, and the aircraft.

The employed Digital Elevation Model (DEM) is a subset of the Advanced Spaceborne Thermal Emission and Reflection Radiometer Global Digital Elevation Model Version 002 (ASTER GDEM V21), developed jointly by the U.S. National Aeronautics and Space Administration (NASA) and Japan's Ministry of Economy, Trade, and Industry (METI), [32].

The ASTER sensor on board of the TERRA satellite, obtained the original model through stereo-correlations of data captured in 2000 and 2011. With a confidence level of 95%, the overall vertically accuracy is of 17 m, while horizontally the resolution is approximately of 75 m.

Nowadays, there is available for download the ASTER GDEM V2 from the Land Processes Distributed Active Archive Centre (LP DAAC) Global Data Explorer (GDEx) [32]. The model is distributed as Geographic Tagged Image File Format (GeoTIFF) files with geographic coordinates (latitude, longitude). The data consists of a 1 arcsecond (approximately 30 m at the equator) grid cell DEM, referenced to the 1984 World Geodetic System (WGS84)/ 1996 Earth Gravitational Model (EGM96) geoid.

Due to the vast area of Azores FIR, it is not possible to do just one DEM for all the islands. However, since most part of the FIR is ocean (no elevation of the terrain), three GeoTIFF files were enough (one with Flores and Corvo Islands, one with Santa Maria and S. Miguel islands, and another one with all the other five islands).

The bilinear interpolation of the DEM matrix is used to extract the profile of the terrain between the ground station and the aircraft. It is expected, for long distances, that most of the path is above the Atlantic Ocean, thus without obstacles, however near the ground station some obstacles can become a

problem. From the transmitting antenna to the receiving one, it is possible to estimate the pair of coordinates (latitude and longitude) of each point and consequently their height above de MSL [30]:

$$\phi_{\mathrm{A-GS,t[rad]}} = \arcsin(\sin(\phi_{GS[\mathrm{rad}]})\cos(t\Delta\theta_{c[\mathrm{rad}]}) + \cos(\phi_{GS[\mathrm{rad}]})\sin(t\Delta_{c[\mathrm{rad}]})\cos(\psi_{A-GS[\mathrm{rad}]})) \tag{3.10}$$

$$\lambda_{\mathrm{A-GS,t}} = \lambda_{GS[\mathrm{rad}]} + \arctan(\sin(\psi_{A-GS[\mathrm{rad}]})\sin(t\Delta\theta_{c[\mathrm{rad}]})\cos(\phi_{GS[\mathrm{rad}]})\cos(t\Delta\theta_{c[\mathrm{rad}]}) - \sin(\phi_{GS[\mathrm{rad}]})\cos(\lambda_{A[\mathrm{rad}]} - \lambda_{GS[\mathrm{rad}]})) \tag{3.11}$$

$$\mathrm{t} \in \left\{t: t \in \mathbb{N}, \mathrm{t} \in [1, \mathrm{N_t}], \mathrm{N_t} = \left\lfloor \frac{\theta_c}{\Delta\theta_c} \right\rfloor\right\} \tag{3.12}$$

$$\Delta\theta_{\mathrm{c[rad]}} = \frac{\Delta d_{DEM[\mathrm{km}]}}{Re_{[\mathrm{km}]}} \tag{3.13}$$

$$\psi_{A-GS[\mathrm{rad}]} = \arctan(\cos(\phi_{A[\mathrm{rad}]})\sin(\lambda_{A[\mathrm{rad}]} - \lambda_{GS[\mathrm{rad}]}) \times \sin(\phi_{A[\mathrm{rad}]})\cos(\phi_{GS[\mathrm{rad}]}) - \cos(\phi_{A[\mathrm{rad}]})\sin(\phi_{GS[\mathrm{rad}]})\cos(\lambda_{A[\mathrm{rad}]} - \lambda_{GS[\mathrm{rad}]}) \tag{3.14}$$

where:

- $\phi_{\mathrm{A-GS,t}}$: t^{th} geodetic latitude sample along a great circle arc;
- λ_A: t^{th} geodetic longitude sample along a great circle arc;
- $\Delta\theta_c$: sampling resolution of the geocentric angle;
- Δd_{DEM}: sampling resolution of the terrain profile;
- ψ_{A-BS}: azimuth of the great circle arc at the aircraft location;
- $\arctan(,)$: four-quadrant inverse tangent.

Of course, for this model to work, it is necessary to know in advanced the position of both terminals (latitude and longitude) and the sampling resolution of the profile.

3.2 Model Implementation

The models presented in Section 3.1 were implemented in a simulator using the matrix-based Math Works MATLAB r2016a language.

3.2.1 Propagation Models

The main purpose of the simulator is to determinate whether there is coverage or not for a given distance between the aircraft and the ground station. This is done by comparing the estimated received power by the terminal with the required one, which depends not only on the transmitting power (predefined) and radiation patterns of both terminals (input parameters) but the path loss too.

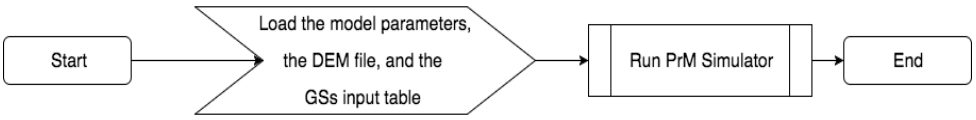

Figure 3-2: Simulator Overview

It is worth noting that the radiation pattern of the ground station antennas comes from an array given by the suppliers. However, for the aircraft, it comes by a nonparametric regression function. For these reasons, in the beginning of the simulation, the digital elevation model (DEM) with a terrain elevation profile matrix must be loaded, as well as the array of the geodetic coordinates of the aircraft and the ground stations, Figure 3-2. It is worth recalling that for the implementation of the Spherical Earth Model the height must be above the Earth Bulge and that the maximum allowed distance in line-of-sight is obtain by applying (2.10).

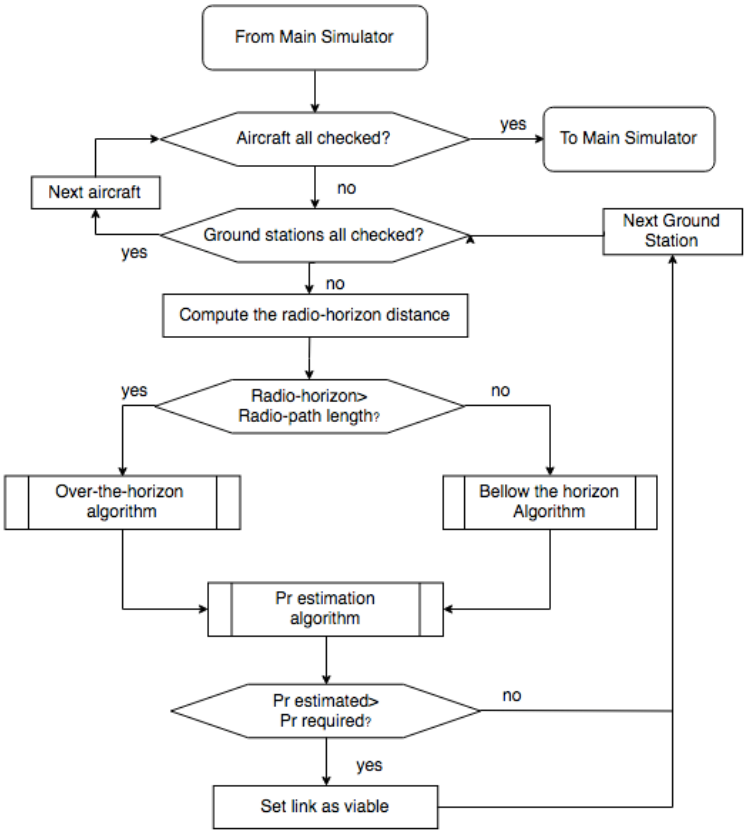

Figure 3-3: Flowchart of the PrM Simulator with the steps required to estimate radio coverage

For this thesis, ones divide the propagation in two: over-the-horizon (when communication is beyond the radio horizon), otherwise, bellow the horizon (Figure 3-3). This happens, because the predominant mechanisms change with the distance, as well as their path losses.

In case of obstruction, the extra attenuation will be estimated through knife-edge Model, in case of a single obstacle, or by Deygout model, in case of multiples (Figure 3-4). The Deygout/knife-edge model function (Figure 3-4) gives the extra attenuation to the bellow the horizon function (Figure 3-5) and, afterwards, it is added to the free-space loss resulting in the total path loss of that link.

Figure 3-4: Flow chart for the Deygout/Knife-Edge Model.

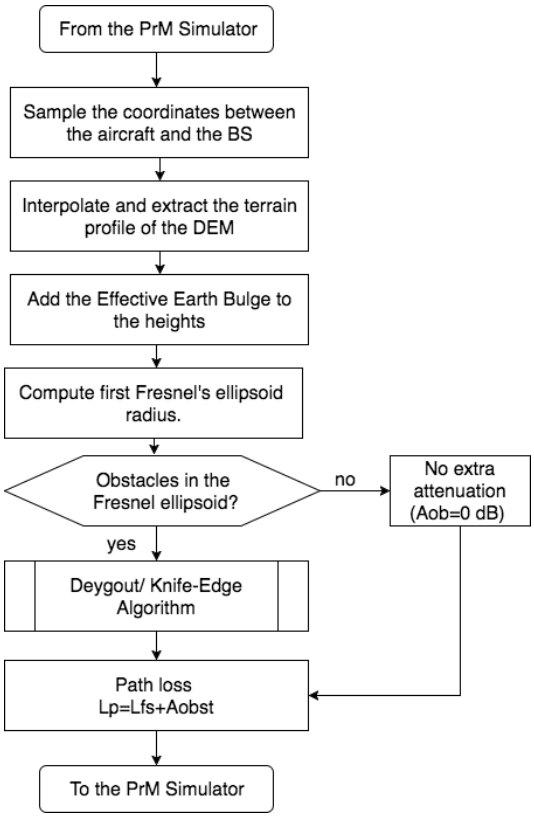

Figure 3-5: Flowchart for the bellow the horizon algorithm.

Over the horizon, the propagation of the signal is due to one of the two following mechanisms:

- Diffraction by Earth's Curvature;
- Tropospheric Scattering.

First, to determinate the path loss of the link for distances over the horizon, the path loss for each mechanism must be estimated.

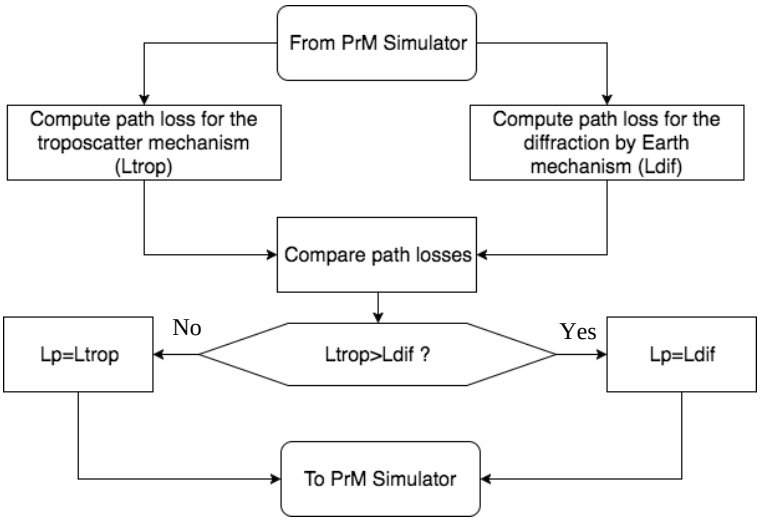

Figure 3-6: Flowchart for the over-the-horizon algorithm.

The mechanism with lower path loss will be the predominant one (Figure 3-6). Estimated the path loss, it is now possible to compute the expected received powerP_r.

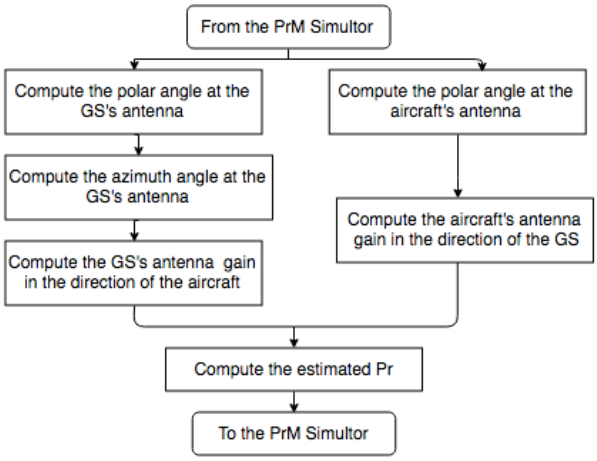

Figure 3-7: Flowchart of the received power estimation algorithm.

In Figure 3-7 the flowchart for the estimation of the received power is represented. As seen in (3.2), the received power depends of both antenna gains, the power of the transmitting antenna and the path loss. The transmitting power is a known value and the path loss has already been estimated. The only unknown factor is then the antenna's gain.

Moreover, to evaluate the troposcattering mechanism, some input parameters are also needed to be load in the beginning of the Main Simulator (Figure 3-2):

- $M = 38.5\,\mathrm{dB}$ (meteorological parameter);
- $\gamma = 0.27/\mathrm{km}$ (atmospheric structure parameter),

and, to evaluate the diffraction mechanism must be loaded:

- σ: electrical conductivity ($\sigma = 5\,\mathrm{S/m}$ for the sea water).

In the case the Ground Station has an omnidirectional antenna, only the elevation gain matters and it can be easily extracted from the gain's matrix. Hence, for directional antennas, the gain is an interpolation of the azimuth and elevation gains, and therefore the azimuth angle needs to be computed (3.15).

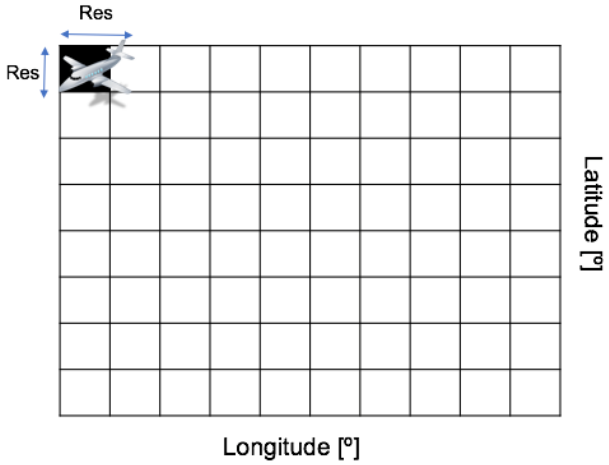

Figure 3-8: Approximated estimation of the total coverage representation.

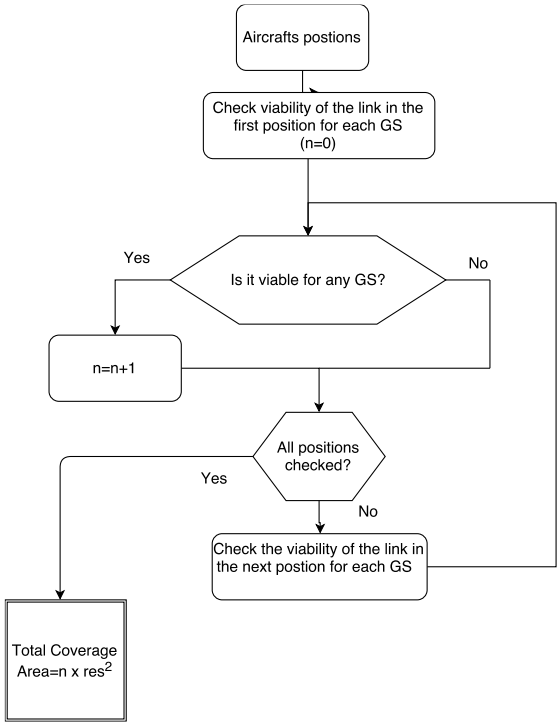

Figure 3-9: Total area coverage estimation.

After having the viability checked for every position and for each GS, the area is now possible to be estimated. Figure 3-8 was drawn in order to help understand how the total area is obtained.

Previously, the simulator saves for each position of the aircraft if the link is viable or not for each GS, where 1 represents that the link is viable and 0 otherwise in a matrix.

3.2.2 Radiation pattern

This section provides the study of the radiation patterns for both GS and the aircraft antennas.

3.2.2.1 Ground Stations

Many times, manufacturers provide the radiation patterns of their designing antenna systems not always in a 3-dimensional way. In fact, the antennas used by NAV have their antennas' radiation pattern split in vertical and horizontal ones, which can be obtained on the website of the manufacturers in .txt format. After extracting both vertical and horizontal radiation patterns, a 3D radiation pattern can be approximated by (3.15).

According to [33], the interpolation method is based on the assumption that both horizontal and vertical radiation patterns of the antenna are available, $G_H(\phi)$ and $G_V(\theta)$. With this information, it is possible to observe that $G_H(\phi)$ has a known range of 2π, with $\phi \in [0, 2\pi[$, as well as $G_V(\theta)$, with $\theta \in [0, \pi[$ for $\phi = 0, \pi$. Calculating the directional gain of the ground station antenna, $G_{GS}(\theta,\phi)$, in any direction $P(\theta,\phi)$, can then be viewed as an interpolation problem, i.e., one wants to obtain the value of a function in a general point, from the knowledge of its value in specific points whose interval contains the general one.

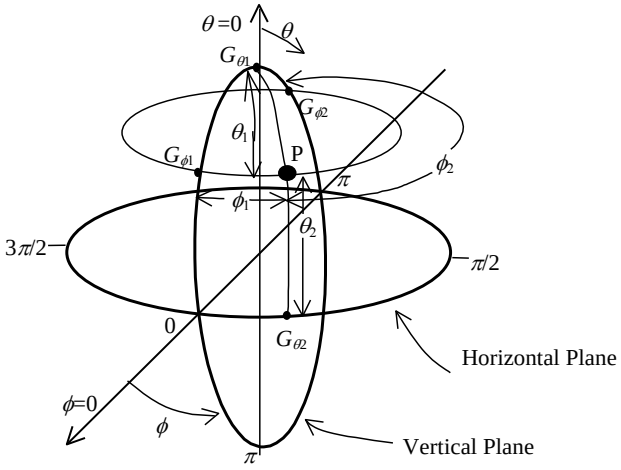

Figure 3-10: Definitions for the interpolation method of the 3-D radiation pattern (extracted from [33]).

Because one is dealing with two coordinates θ and ϕ, this can be solved as a 2-D problem and, to help visualize the problem, it is helpful to map the surface of the sphere onto a planar surface, defined by the two coordinates (Figure 3-11):

- The north and south poles of the sphere, $\theta = 0$ and $\theta = \pi$, correspond respectively to the upper and lower horizontal lines, in which the directional gain is know from the vertical cut, $G_{\theta 1} = G_V(\theta = 0)$ and $G_{\theta 1} = G_V(\theta = \pi)$ (the same notation is used, since the point of interest never uses both values in the interpolation, and either one or the other is used);

- the central horizontal line corresponds to the equator, $\theta = \pi/2$, on which the horizontal cut of the radiation pattern is defined and known, $G_{\theta 2} = G_H(\phi)$;
- the left and right vertical lines correspond to different representations of the same meridian, $\phi = 0$ or $\phi = 2\pi$, which is associated to the half of vertical cut in the (usually defined as) forward direction of the antenna, $G_{\phi 1} = G_V(\theta, \phi = 0)$;
- the central vertical line corresponds to the meridian $\phi = \pi$, which is associated to the half of vertical cut in the (usually defined as) backward direction of the antenna, $G_{\phi 2} = G_V(\theta, \phi = \pi)$.

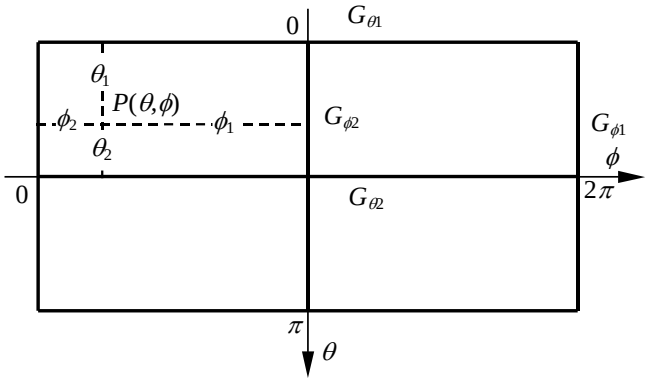

Figure 3-11: Mapping of the sphere's surface onto a planar surface (extracted from [33]).

A final formulation for the interpolated directional gain in any direction $P(\theta,\phi)$ is obtained by [33]:

$$G_{GS} = \frac{\left[\phi_1 G_{\phi 2} + \phi_2 G_{\phi 1}\right]\frac{\theta_1\theta_2}{(\theta_1+\theta_2)^2} + \left[\theta_1 G_{\theta 2} + \theta_2 G_{\theta 1}\right]\frac{\phi_1\phi_2}{(\phi_1+\phi_2)^2}}{\left[\phi_1 + \phi_2\right]\frac{\theta_1\theta_2}{(\theta_1+\theta_2)^2} + \left[\theta_1 + \theta_2\right]\frac{\phi_1\phi_2}{(\phi_1+\phi_2)^2}} \tag{3.15}$$

The study made by [33] concluded that this interpolation method can be quite accurate, and very helpful on the estimation of 3-D antennas' radiation patterns for the usage of propagation simulation tools.

The polar angle between the direct ray and the vertical plane on the ground station is given by [30]

$$\theta_{GS[rad]} = \sin^{-1}\left(\frac{\Delta h^A_{GS[\mathrm{km}]}}{d_{[\mathrm{km}]}}\left(1 - \frac{\Delta h^A_{GS[\mathrm{km}]}}{2\, r_{GS[\mathrm{km}]}}\right) - \frac{d_{[\mathrm{km}]}}{2\, r_{GS[\mathrm{km}]}}\right) \tag{3.16}$$

where:

- θ_{GS}: polar angle on the ground stations antennas.

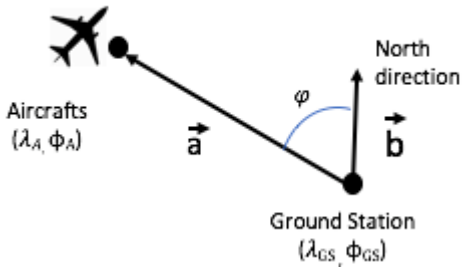

Figure 3-12: Azimuth angle representation.

In case of directional antennas, the gain of the antenna does not only varies vertically but also horizontally. As presented in Figure 3-12 , φ represents the horizontal angle, between the direction of maximum radiation and the azimuthal position of the aircraft.

Considering that antenna is pointed to the North Pole, represented by the $\vec{b}$ vector in

Figure 3-12, and a vector $\vec{a}$ with the origin on the ground coordinates and end in the aircrafts position the azimuth angle can be determined by:

$$\varphi = \operatorname{acos}\left(\frac{\vec{a} \bullet \vec{b}}{ab}\right) \tag{3.17}$$

where:

- a: magnitude of the vector $\vec{a}$;
- b: magnitude of the vector $\vec{b}$.

3.2.2.2 Airborne

As for the aircraft, [31] recommends that the transponder antenna system installed on an aircraft should has a radiation pattern nominally equivalent to that of a quarter-wavelength monopole on a ground plane, however, in reality, because of reflection, refraction and dispersion effects caused by the structure of the aircraft, the radiation pattern can vary for different positions or even from aircraft to aircraft. Therefore, the estimated gain is never truly accurate.

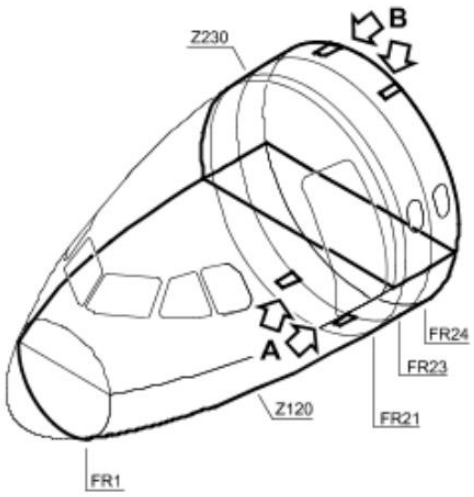

Figure 3-13: Aircraft's fuselage transversal cut showing transponder antennas locations (extracted from [30]).

There is a total of four antennas in a typical commercial aviation aircraft: two on the bottom (pointed as A in Figure 3-13) and the other two on top of the fuselage (pointed as B). To provide omnidirectional coverage for lower and upper airspace, the antennas commonly are set in the front of the fuselage and normally the antennas are either planar or wire monopoles 42 encapsulated on a blade shaped dielectric to provide protection and minimise aerodynamic drag [30]. For this master thesis, the antenna is assumed to be a wire monopole seated on the lower fuselage, forward of the wings.

With the purpose of obtaining an estimated trustworthy radiation pattern for the aircraft, [30] designed a quarter wavelength wire monopole in Antenna Magus. Afterwards, in CST Microwave Studio through some steps were simulated far-field results which could be then exported to MATLAB. These far-field results obtained by [30] are used for the simulation scenario.

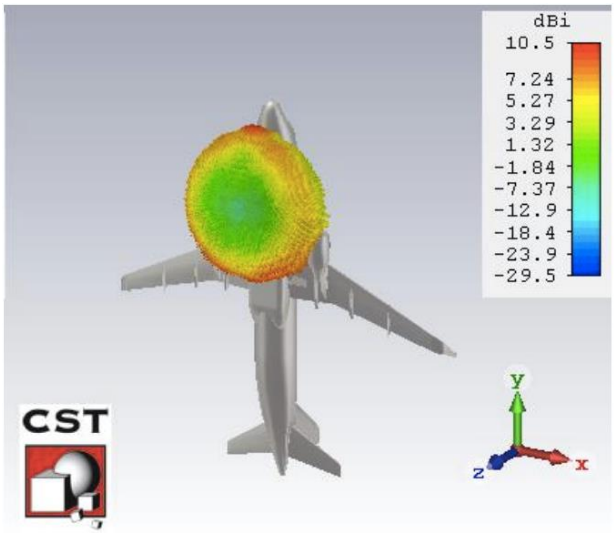

Figure 3-14: Representation of the aircraft's antenna near-field (extracted from [30]).

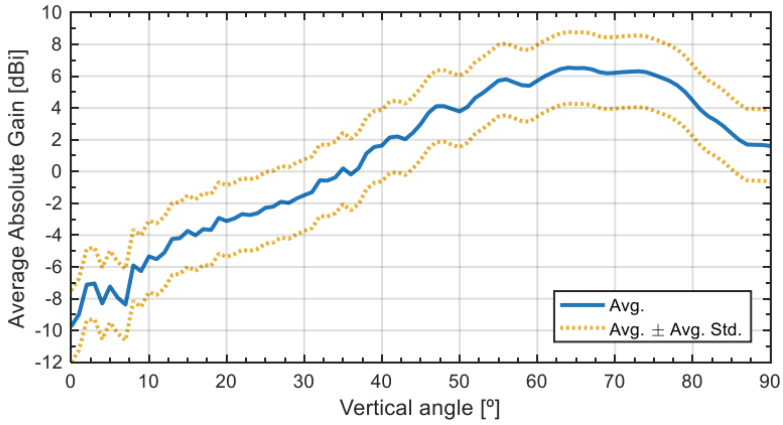

Figure 3-15: Average absolute transponder antenna gain, with 2.25 dBi average standard deviation (extracted from [30]).

Since the gain varies with the position of the aircraft due to the aero structure, and due to the accuracy of the far field results obtained and represented in Figure 3-14, averaging the 3D far-field pattern simulation along the horizontal angle for each position of the vertical one, results in an average absolute gain for the vertical angle as shown in Figure 3-15, with an average standard deviation of 2.25 dBi.

The polar angle between the direct ray and the vertical plane on the aircraft's antenna can be estimated by [30] :

$$\theta_{A[rad]} = \sin^{-1}\left(\frac{\Delta h^{A}_{GS[\mathrm{km}]}}{d_{[\mathrm{km}]}}\left(1 - \frac{\Delta h^{A}_{GS[\mathrm{km}]}}{2\, r_{A[\mathrm{km}]}}\right) - \frac{d_{[\mathrm{km}]}}{2\, r_{A[\mathrm{km}]}}\right) \tag{3.18}$$

where:

- θ_A: polar angle on the aircraft.

3.3 Model Assessment

The validation of the models implemented in the simulator described in the Section 3.2 is the focus of this section.

Table 3.1: Validation of the simulator.

Test	Description
1	Check if the path loss variates well with the distance.
2	Verify if the profile of the terrain is taken into consideration as well as the Fresnel ellipsoid and direct ray.
3	Verify if the 2D and 3D radiation patterns of the antennas are similar to the theoretical ones.
4	Assess the received power by the aircraft and the GS
5	Verify if the estimated coverage in Azores' is similar to the one given by NAV Portugal.

Table 3.1 summarize the fundamental points to be assessed. This is done by comparing the outputs from the simulator with previously well-known behaviours. Only after that, it can be ensured that the simulator is reliable to provide useful information.

Table 3.2: Parameter assumptions.

Parameter	Value assumed
Aircraft's Gain [dBi]	1
Ground Station Gain [dBi]	2.15
Frequency [MHz]	127
Aircrafts P_{EIRP} [W]	50 [6]
GS P_{EIRP} [W]	44
Aircraft's height	FL300 (9144 m)
GS's height [m]	959
Aircraft's E_{rmin} [μV/m]	30
GS's E_{rmin}[μV/m]	20

Table 3.2 presents the assumption necessary to test the simulator.

The final purpose of the simulator is to give the total coverage estimation. Knowing that the strength of the received signal depends on the path loss, gains of the transmitter and the receiver, as well as the transmitting power, these are then the parameters that must be assessed in order to test whether it gives at the end trustworthy coverage estimations.

Losses in the pathway are something unavoidable. If the distance between the aircraft and the VHF ground station does not go beyond the radio horizon, it is expected that the radio wave propagates in LOS. Of course, that in case of having some considerable obstacles in the path, the strength of the signal can lose a part of its strength.

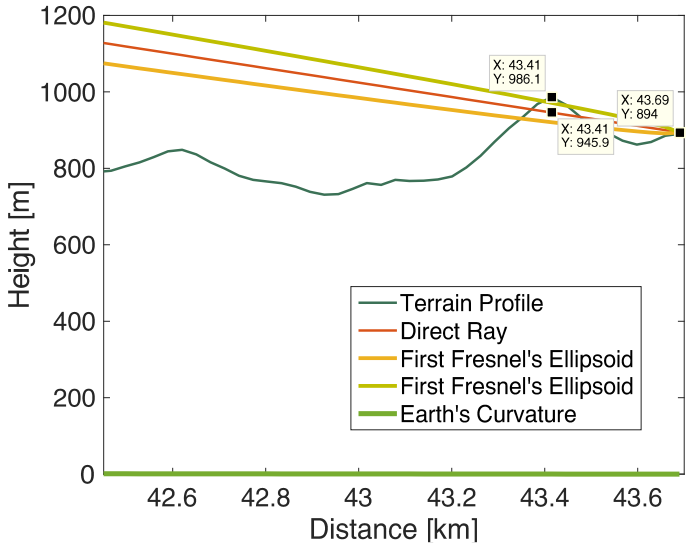

Figure 3-16: Radio line-of-sight assessment with a considerable obstacle.

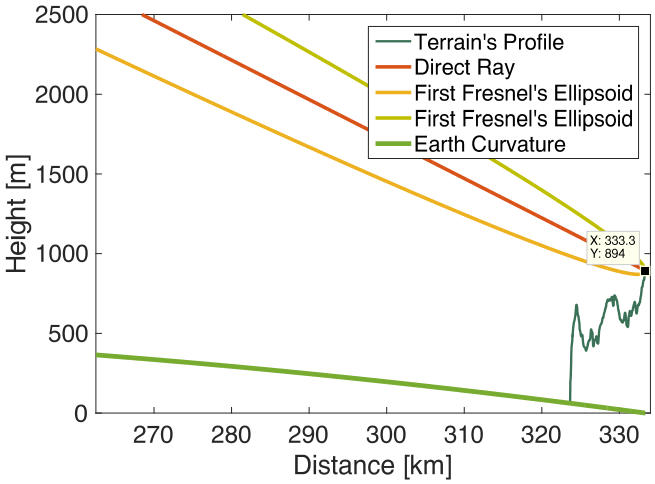

Figure 3-17: Radio line-of-sight assessment without any considerable obstacle.

The propagation models that must be evaluated are the free space, the deygout/knife-edge, the diffraction through Earth's curvature and the tropospheric scattering models. One can see in Figure 3-16, the first Fresnel's Ellipsoid as well as the direct ray between the aircraft and the ground station

and the terrain profile. Worth noting that the curvature of the Earth is taken into account and there are considerable obstructions of the direct ray between the aircraft at 39° 35' 25.23"N, 31° 41' 26.52" W and the ground station antenna located in Morro Alto, Flores.

Nevertheless, in Figure 3-17. there are no obstacles when the aircraft passes at 36° 27' 47″ N, 31° 13' 10″ W point and the communication is made in line-of-sight and the simulator, as expected, confirmed that there is no extra attenuation due to the terrain profile.

Bellow the horizon, diffraction can be used to establish communication at short distances. But as the propagating distance increases, the path loss increases rapidly and beyond a certain distance, scattering due to tropospheric irregularities are much more important than diffraction. This is due to the signal fading of scattering being relatively slow as the distance increases compared to high signal fading due to diffraction.

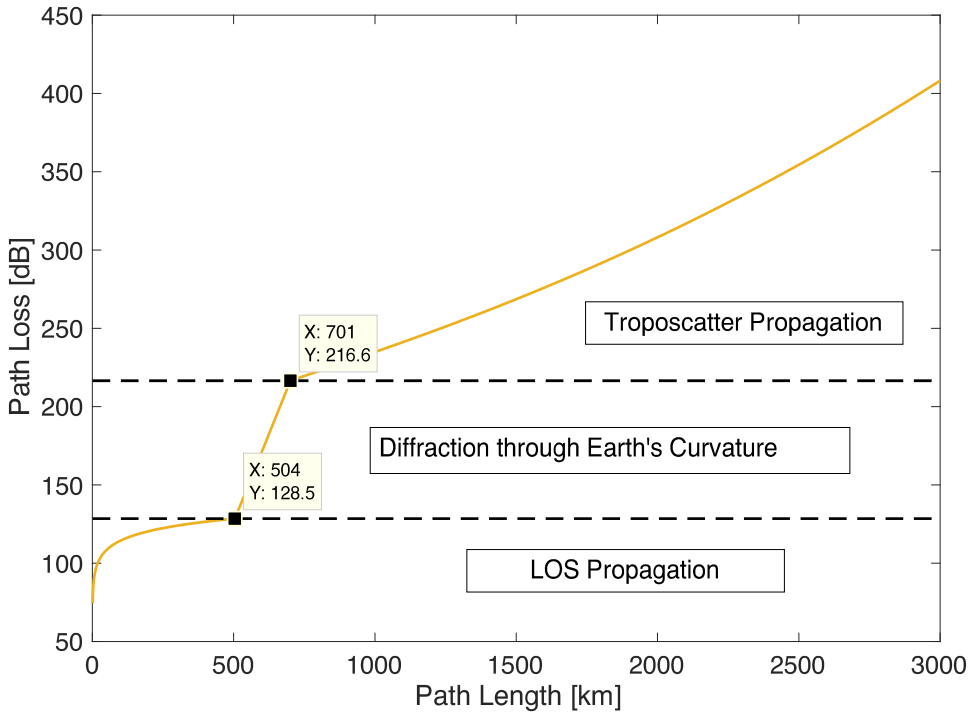

Figure 3-18: Path Loss for different propagation mechanisms.

With the assumptions described in Table 3.2 and with the models implemented and described in Section 3.2.1, ones obtained a graph where it can be seen how the path loss variates with the distance. Worth noting that, as foreseen, after the radio horizon, diffraction in the Earth's curvature predominates and the path loss increases drastically until the troposcatter mechanism overcomes.

Table 3.3: Numerically calculated parameters.

Parameters	Value
Line-of-sight distance [km]	521.79
Penumbra width [km]	37.68
Transition from light to shadow distance	502.95

With the help of Figure 3-18 and

Table 3.3, it is possible to observe that the simulator gives reliable results. A little bit before the radio horizon, the predominant mechanism is already the diffraction by the Earth's curvature supporting theoretically the fact that close to that distance, a great part of the Fresnel first ellipsoid is obstructed by the Earth itself (shadow zone). Also, it is possible to observe how the path loss in the troposcatter is relatively slow as the distance increases when in comparison with the one due to diffraction.

One of the inputs of the simulator is the radiation pattern of the ground stations' antennas. NAV currently uses both omnidirectional and directional antennas. One example is the collinear omnidirectional array antenna used in S. Miguel with a maximum gain of 0 dBd, i.e., 2.15 dBi, whereas for a directional antenna it is a 3 elements Yagi with a maximum gain of 7.8 dBi. The maximum gain occurs for a polar angle of θ=90º to favour the links close to the radio horizon where attenuation is more intense.

Afterwards, setting the antenna in the middle of the ocean, without obstacles nearby, it is done a coverage analysis to evaluate the accuracy of the simulator relatively to the coverage, i.e., whether coverage is omnidirectional or not, and if it covers a reliable distance. The same procedure is done for a Yagi 3 elements' directional antenna to assess the simulator for directional antennas.

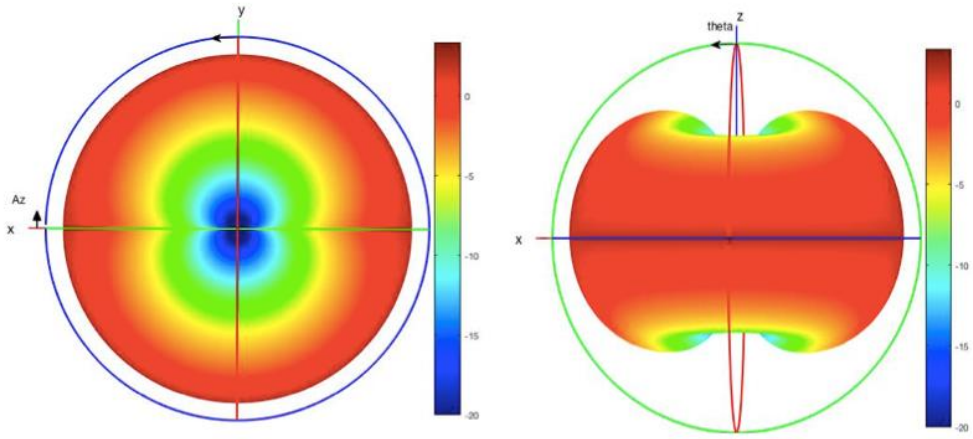

(b) Horizontal view (a) Vertical view

Figure 3-19: Horizontal and Vertical views of the SC272 Omnidirectional Array interpolated gain (G_{max}=2.15 dBi).

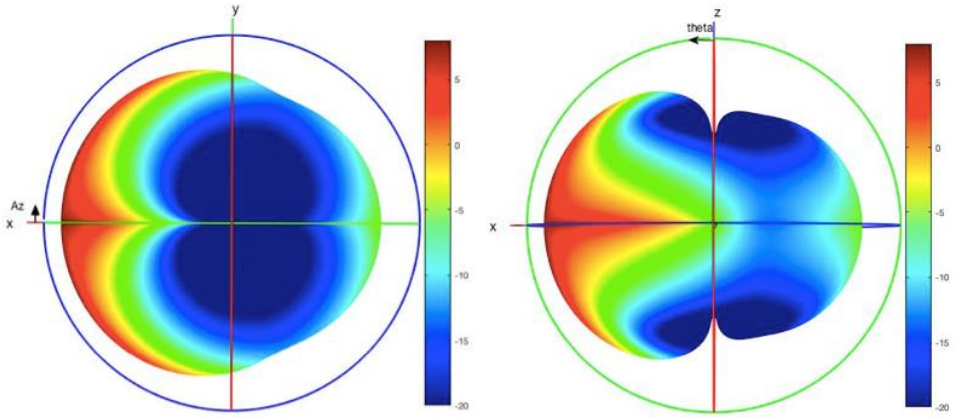

(b) Horizontal view (a) Vertical view

Figure 3-20: Horizontal and Vertical views of the Yagi 3 elements' interpolated gain (G_{max}=7.8 dBi).

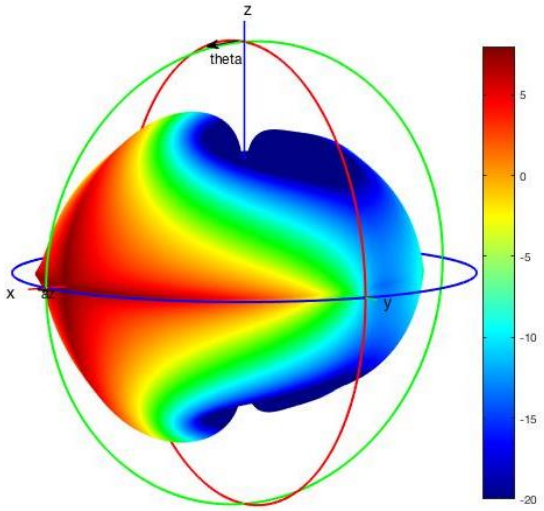

Figure 3-21: 3D representation of the interpolated gain for the Yagi 3 elements' Antenna.

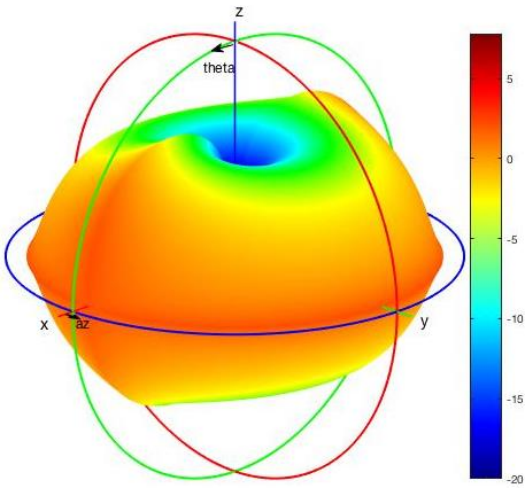

Figure 3-22: 3D representation of the interpolated gain for the SC272 Omnidirectional array.

With help of MATLAB R2016b, the Figure 3-19 and Figure 3-20 deploys both vertical and horizontal planes for both omnidirectional array and for the 3 elements' Yagi antenna currently used by NAV. As for the 3D representation of these antennas, shown in Figure 3-21 and Figure 3-22, is used the approximated interpolated equation presented in (3.15).

For the power assessment, the total path loss obtained previously and represented in Figure 3-18 is going to be considered. It is now possible to observe, in Figure 3-23 and Figure 3-24 that its received power decreases as the path loss increases and the coverage ends with the diffraction of the Earth's curvature. Of course, in cases of obstruction bellow the horizon, the coverage will be shorter than the one represented whereas for higher gain antennas' the coverage must increase.

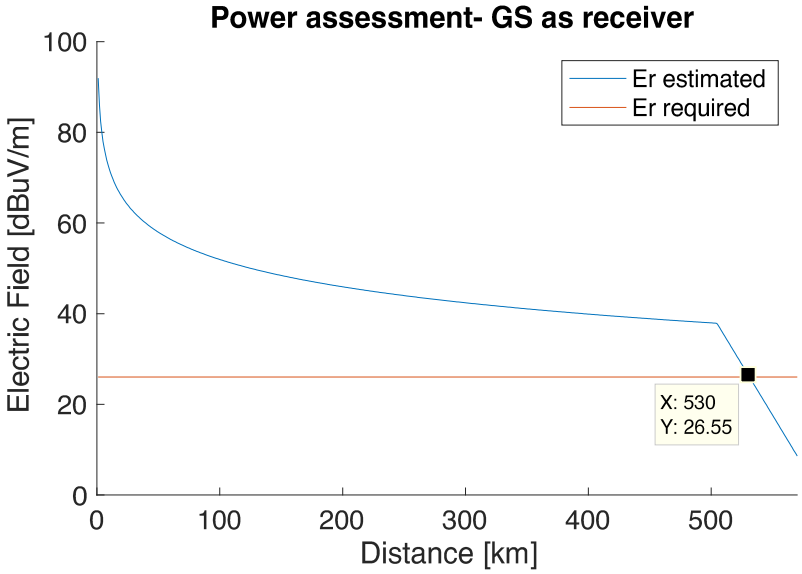

Figure 3-23: Power Assessment- GS as Receiving Antenna.

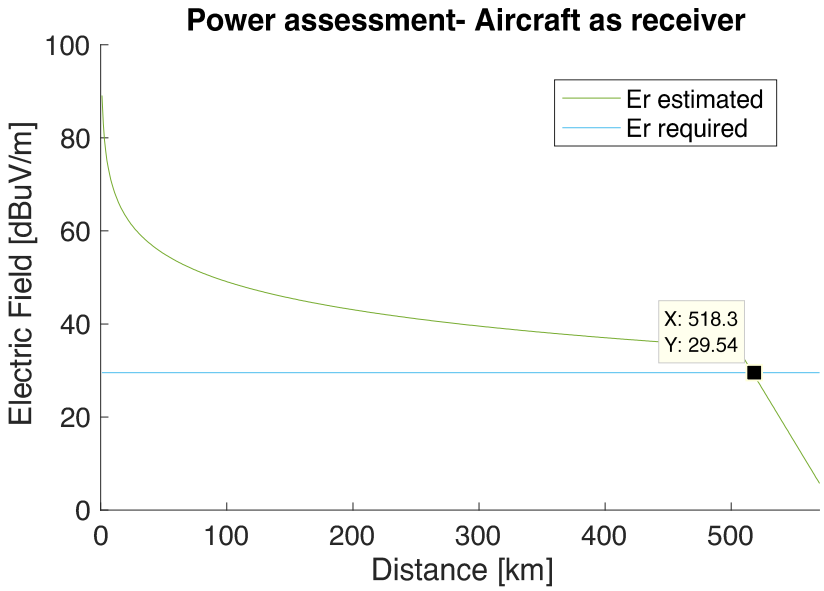

Figure 3-24: Power Assessment- Aircraft as Receiving Antenna.

Lastly, a comparison between the coverage given by NAV (Figure 3-25) is done with the one obtained by the simulator. However, it is worth noting that, in Figure 3-25, not all the antennas are VHF ones and their coverage is only used to help comparing with the ones obtained by the simulator and their location may be also outdated. Even though the radar antennas are in VHF, they only work in line-of-sight therefore, in case of having any obstructions that area is not covered. Special attention to the GS antenna in Figure 3-25, in Porto Santo which is a VHF radar, with omnidirectional coverage while for one simulated (Figure 3-26) it is used an array with two 3 elements' Yagi (G_{max}=9 dBi), pointed directly to Santa Maria (φ=310º). The differences can come by the fact that even though propagation is not in LOS, the received power can be enough for the receiver to listen the message properly.

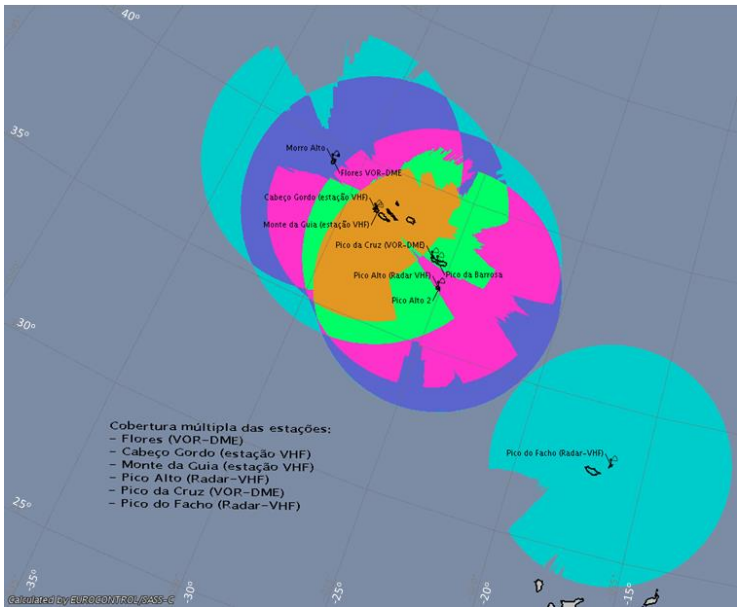

Figure 3-25: Estimated coverage of Azores' FIR given by NAV Portugal (adapted from [4]).

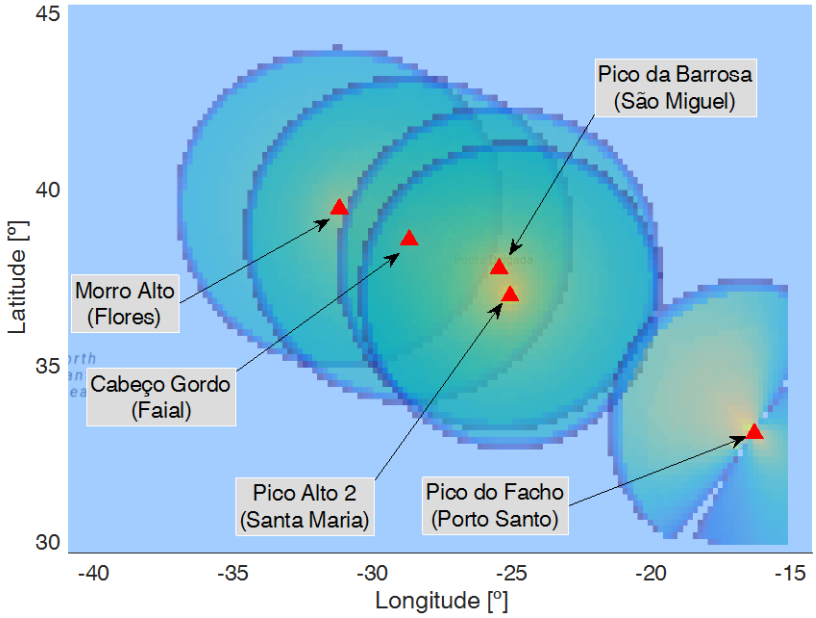

Figure 3-26: Estimated coverage of Azores' FIR given by the simulator.

The best-case scenario would be to cover the whole Santa Maria's Oceanic FIR with a total area of 5 138 160.886 km², i.e., 1 496 134 NM², however, this is not possible. The percentage of coverage area can be obtained by (3.19):

$$S_{[\%]} = \frac{A_{cov[\mathrm{km}^2]}}{A_{FIR[\mathrm{km}^2]}} \times 100\% \tag{3.19}$$

where:

- S: Percentage of the covered area in the Azores' Oceanic FIR;
- A_{FIR}: FIR's total area of 1 496 137 NM²=5 138 160.886 km²;
- A_{cov}: Estimated coverage area.

Figure 3-27 represents an overlapping of Figure 3-25, Figure 3-26 and Figure 1-2 in Photoshop. Finally, the calculation of the total coverage, for a resolution of 20 km, is of 2 298 400 km² = 669 250 NM², which, using (3.19), covers only 44.73% of the FIR.

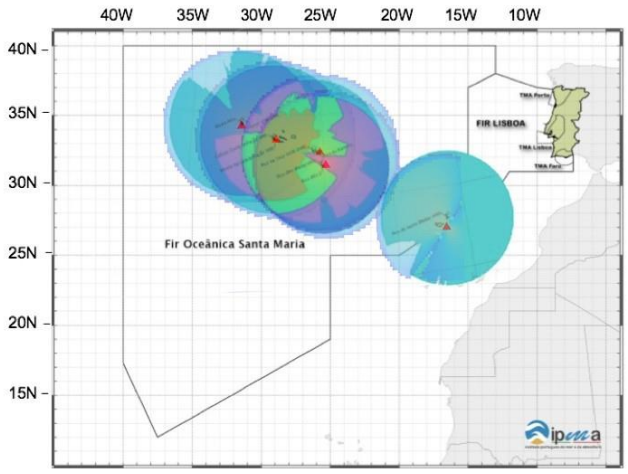

Figure 3-27: Comparison of the coverage estimated by the simulator and the one given by NAV.

Chapter 4

Model Development

This chapter provides the description of the scenarios for the performance analysis, and the analysis of solutions and of their implementation. The chapter starts with the description of the GSs and simulation parameters for the scenarios under study. The chapter ends with the results from the model for the scenarios under study.

4.1 Actual coverage scenario

Figure 4-1 shows the locations of the VHF GSs in the Azores' FIR superimposed with a map from Google Earth maintained by NAV Portugal.

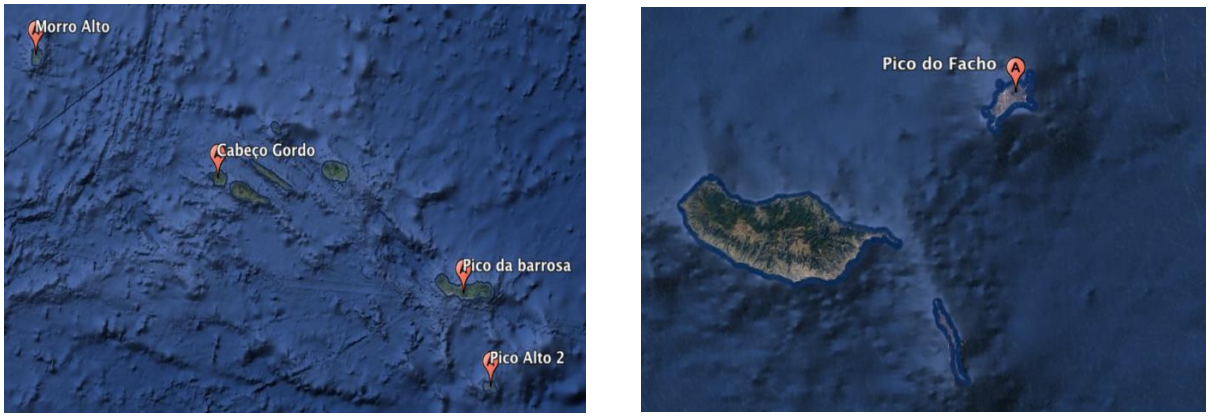

(a) Azores (b) Madeira

Figure 4-1: Locations of the GSs in Azores' FIR.

The information related to all the VHF ground station antennas in Azores' FIR can be find in Table 4.1.

Table 4.1: Information about the VHF ground station antennas of NAV.

Location	Coordinates	Height [m]	Radiation Pattern	Gain [dBd]	EIRP [W]
Morro Alto (Flores Island)	39° 27' 48,28 N 31°13' 11,68" W	3	Omnidirectional	-1.1	33
Pico da Barrosa (S. Miguel Island)	37° 45' 35" N 25° 29' 27" W	20	Omnidirectional	0	40
Pico Alto 2 (Santa Maria Island)	36° 58' 58,50" N 25° 05' 27,30 W	10	Omnidirectional	0	45
Cabeço Gordo (Faial Island)	38° 34' 33" N 28° 42' 45" W	3	Omnidirectional	-1.1	48
Pico do Facho (Porto Santo Island)	33° 05' 03,0 N 16° 19' 28,9 W	15	Directional	9	250

The heights in Table 4.1 are referred to the GSs ones. Moreover, it is described which antenna is used for each GS as well as their radiation pattern and maximum gain. More information related to these antennas can be found in Annex A.1, A.2 and A.3.

To use the propagation models correctly, it must be added to the antenna's height, the profile of the terrain in that location (Table 4.2).

Table 4.2: Heights of the terrain profile and consequently, of the GSs above mean sea level.

Location	Terrain Profile [m]	GS Height AMSL [m]
Morro Alto	890.97	893.97
Pico da Barrosa	939.31	959.31
Pico Alto 2	571.50	581.50
Cabeço Gordo	1010.67	1013.67
Pico do Facho	470	485

As for the aircraft, the elevation pattern obtained in Section 3.2.2.2 is represented in Figure 4-2.

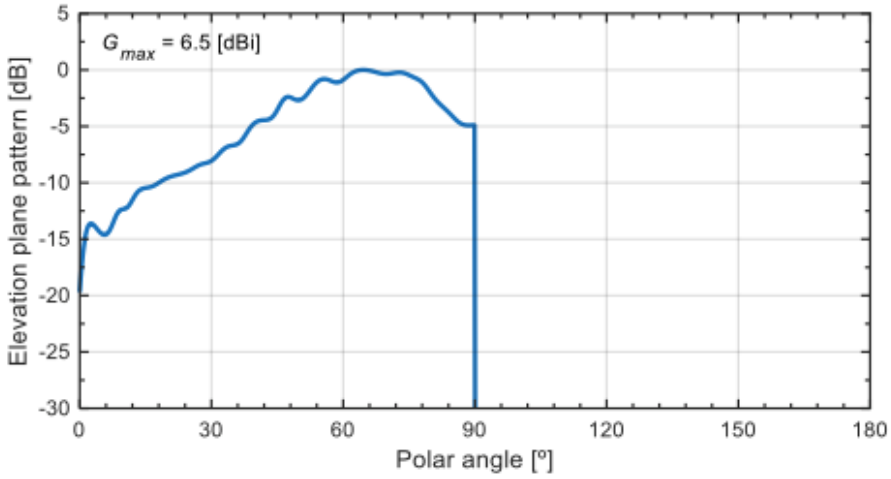

Figure 4-2: Elevation plane pattern for the aircraft.

The controlled airspace can be divided in two air routes: the upper and the lower ones. The upper air routes (UARs) sit above airways (above FL245) and it is the one that matters for this thesis.

As for the elevation pattern of the aircraft, it is depicted in Figure 4-2.

A TMA, as previously said, is the designated area of controlled airspace surrounding a major airport where there is a high volume of traffic. In Azores' TMA, shown in Figure 1-2, aircrafts in route normally are at FL245, and for this reason, one must ensure that there is also coverage when flying at that altitude (worst case scenario). On the other hand, when the aircraft is far from the TMA, it usually flies at FL300 or higher. Therefore, one must also evaluate both cases as favourable case scenarios.

It is also worth noting that multipath will be considered insignificant and for that reason there is no fading margin.

4.2 Coverage Improvement

In this section is presented the study on the improvement of coverage in case of changing the antennas already implemented (Table 4.1) with other with higher gains.

Until the radio-horizon, the already implemented antennas are enough, and even though collinear omnidirectional antennas have higher gains compared with the implemented ones, it is not enough of to propagate the signal beyond the horizon; for this reason, high gain directive antennas must be studied. It should be taken into account, when locating the antennas, whether the aircraft suffers from interference. NAV Portugal uses only three frequencies for aeronautical voice communication and one must use for this thesis also a maximum of three. Figure 4-3 presents, through different colours, how many ground stations are covering a certain area:

- Yellow: Only one GS covers that particular area;
- Blue: Two GS cover that particular area;
- Green: Three GS covers that particular area,

As it is possible to observe, there's a maximum of 3 GS's coverage overlapping the same area. Therefore, when defining the location of the new GS that one is going to implement and to where to point horizontally, that overlapping must be taken into consideration.

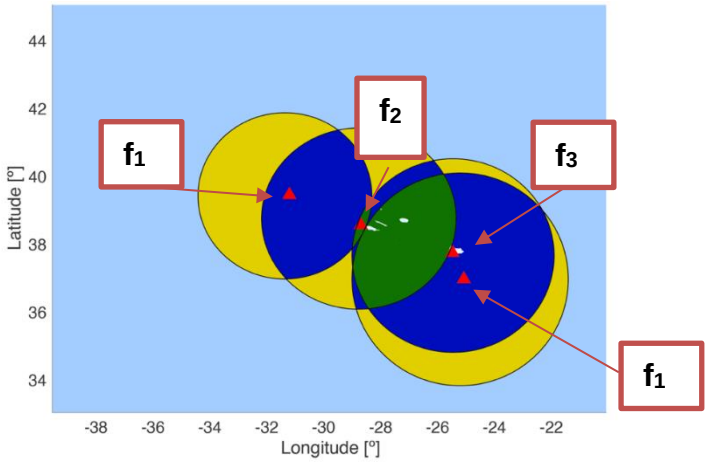

Figure 4-3: Representation of overlapping coverage for aeronautical communication services.

Therefore, Faial's GS antenna needs to have an operating frequency band different from the one in Flores as well as the one in S. Miguel. Santa Maria's GS antenna and the S. Miguel's cannot have the same working frequency band. So, in order to reduce interference, as pointed out in Figure 4-3, Faial's and Santa Maria's GS antennas can operate with the same frequency band and Faial's and S. Miguel's need to be different from the other two.

Skymasts Manufacturer presents three relevant types of Yagi antennas with larger gains. These are the 6 elements' Yagi antenna [35], with a gain of G_{max}=10.65 dBi, the 12 elements' Yagi [36] with a gain of G_{max}=14.15 dBi and an 18 elements' Yagi [37] with G_{max}=16.35 dBi. All figures were developed by MATLAB R2016b. More elements represent a higher forwa gain, more side lobes and smaller Half Power Beam Width (HPBW). Also, with the help of MATLAB R2016b, the vertical and horizontal planes

of the radiation pattern as well as their approximate 3-D radiation pattern are displayed in Figure 4-4, Figure 4-5, Figure 4-6, Figure 4-7, Figure 4-8 and Figure 4-9.

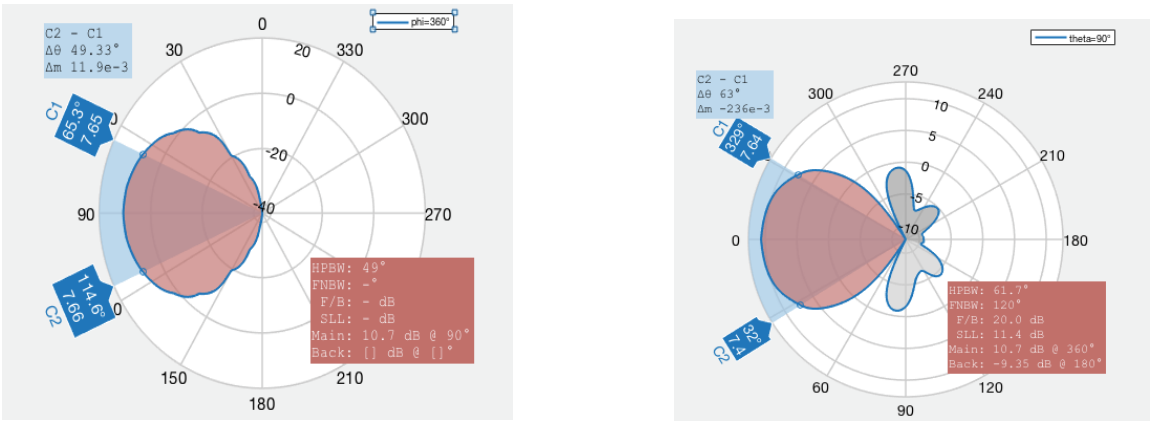

(a) E-Plane (b) H-Plane

Figure 4-4: E and H-Plane for Yagi 6 elements' antenna.

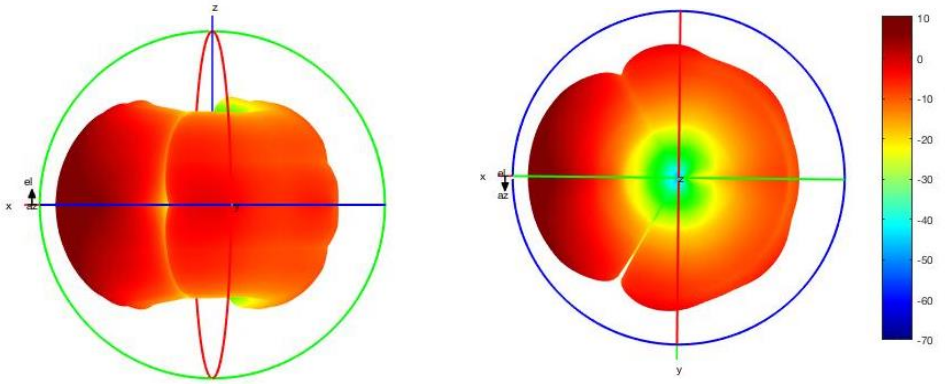

(a) Vertical View (b) Horizontal View

Figure 4-5: 3D interpolated Radiation pattern for Yagi 6 elements' antenna.

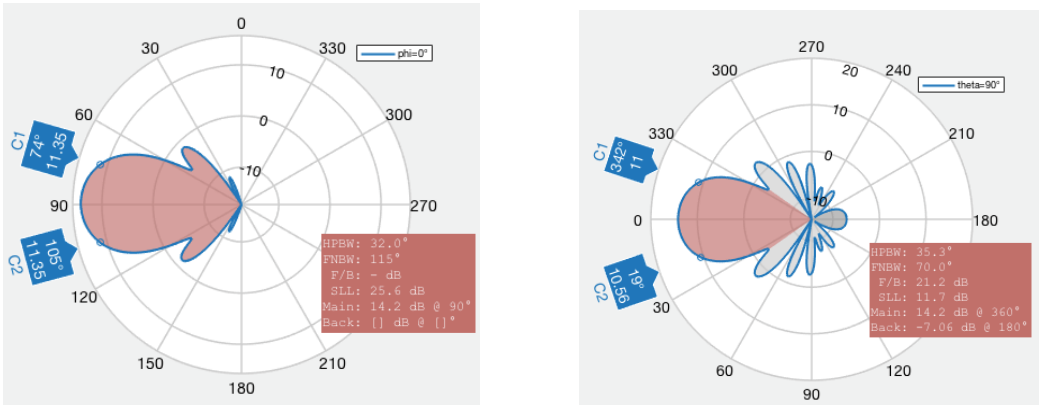

(b) E-Plane (b) H-Plane

Figure 4-6: E and H-Plane for Yagi 12 elements' antenna.

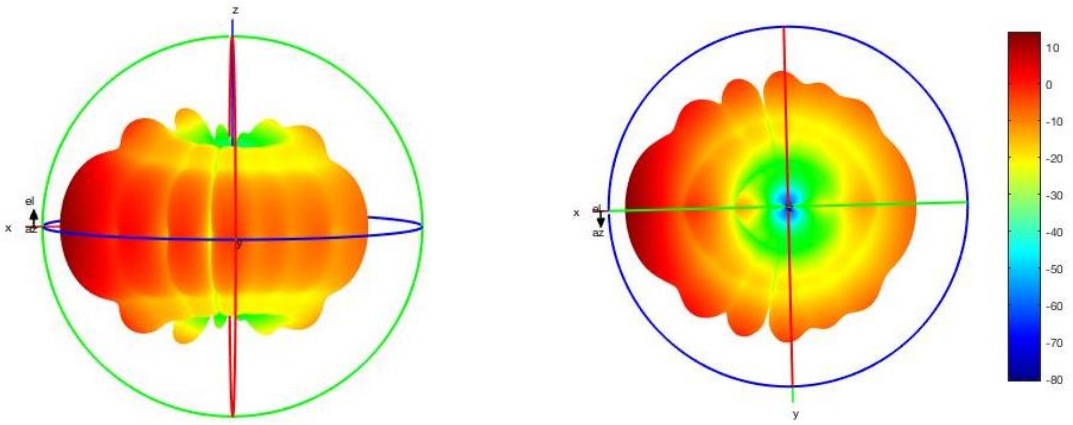

(b) Vertical View (b) Horizontal View

Figure 4-7: 3D interpolated Radiation pattern for Yagi 12 elements' antenna.

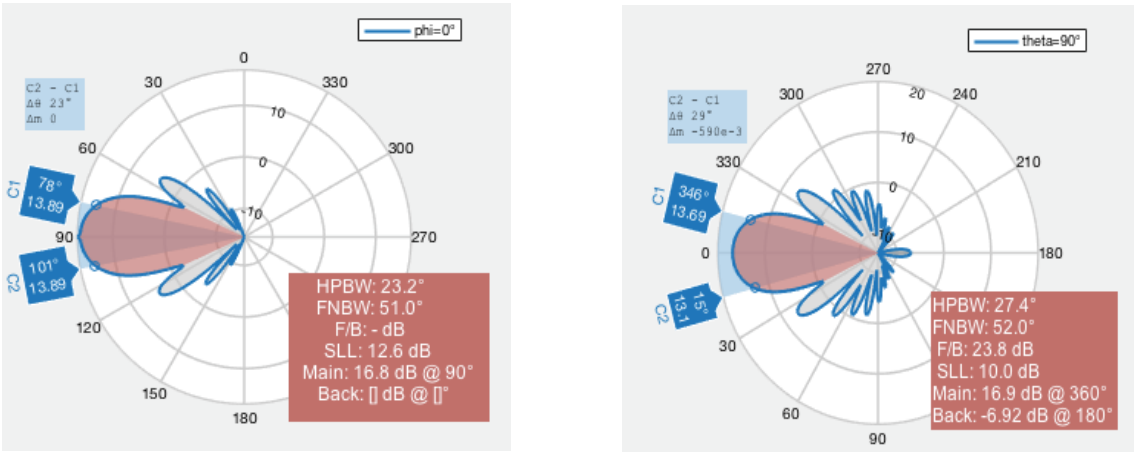

(c) E-Plane (b) H-Plane

Figure 4-8: E and H-Plane for Yagi 18 elements' antenna.

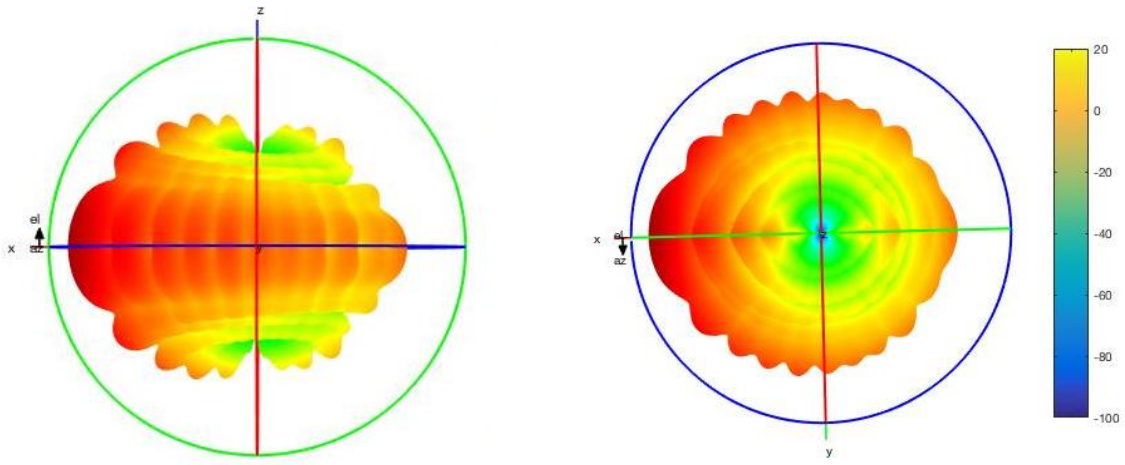

(c) Vertical View (b) Horizontal View

Figure 4-9: 3D interpolated Radiation pattern for Yagi 18 elements' antenna.

The first step, to understand whether these antennas are adequate for this thesis, is to estimate the improvement of coverage compared to the ones already implemented. It is also necessary to calculate if the communication still works really near the GS antenna, where the gain is negligible.

Figure 4-10: Path representation to analyse the coverage length in Morro Alto, Flores.

Figure 4-10 defines the trajectory of the aircraft that is studied in Figure 4-11. Note that it is defined as negative distances when the aircraft is on the south side of the GS and positive when it is north, i.e., the aircraft flies north. Figure 4-11 represents the coverage for each type of antenna located at the same geographic coordinates as the one implemented in Morro Alto, Flores (h_{GS}=859 m) with the aircraft at a FL245 (the minimum height possible in the upper space) which, of course, for higher FL the coverage improves. This fact must be taken into consideration when whether there is enough power for the pilot to receive the signal from the GS properly.

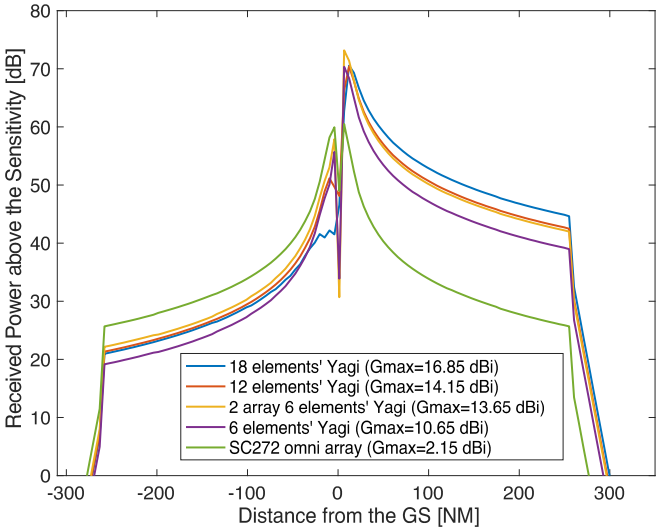

Figure 4-11: Coverage for each antennas' type when the aircraft is flying South->North (FL245).

Figure 4-11 assures that there is no poor communication when the aircraft comes close to the GS, so, there is no need to retune the frequency in this situation, even for the more directive antennas

. Relevant information regarding Figure 4-11 is that:

- The SC272 antenna array covers 278 NM (≈515 km);
- There is coverage of the Yagi 6 elements' Antenna is up to 293 NM (≈543 km);
- The 2 array Yagi 6 elements' antenna increases the coverage to 296 NM (≈549 km);
- The 12 elements' Yagi covers up to 298 NM (≈551 km);
- Lastly, the 18 elements' Yagi coverage goes up to 299 NM (≈555 km).

However, the extension of coverage is not the only thing that improves. Another important feature of using more directive antennas is the fact that for distances close to the horizon the received power is greater. Comparing these Yagis with the SC272 omnidirectional one, near the horizon, the received power elevates more than 10 dB, i.e., ten times more. The non-symmetrical behaviour in Figure 4-11 is expected, since the front-back ratio of the Yagi antennas is considerable.

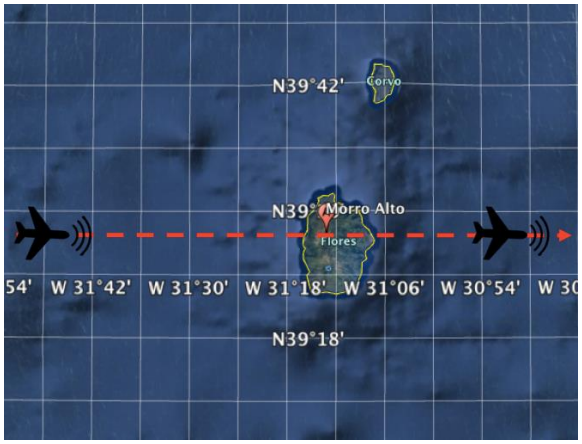

Figure 4-12: Aircraft's route flying from West to East.

Figure 4-12 presents the route when the aircraft is communicating with the pilot through the GS in Morro Alto, Flores when the aircraft is flying from west to east.

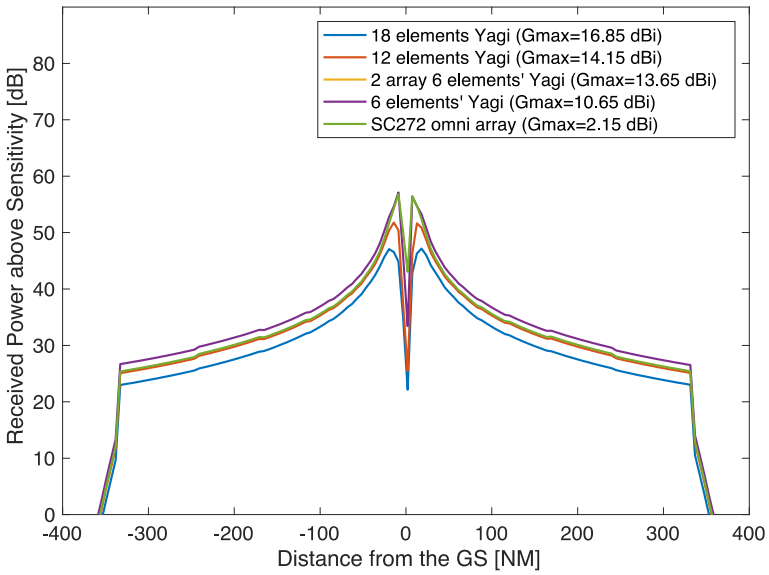

Figure 4-13: Coverage for each antennas' type when the aircraft is flying West>East (FL245).

Figure 4-13 presents the maximum distances when the aircraft is flying west to east and the GS antenna is pointing north. There are no significant obstacles obstructing the link between the receiving and

transmitting antennas therefore the coverage distance is a bit longer than the one in Figure 4-11. Of course, since the radiation pattern is symmetrical and contrary to the one presented in Figure 4-11, it is expected for the received power to be also symmetrical. Little differences come due to link obstructions.

Studied the coverage close to the GS, where the aircrafts fly at lower heights, ones must study now the realistic coverage above the horizon where they fly much higher.

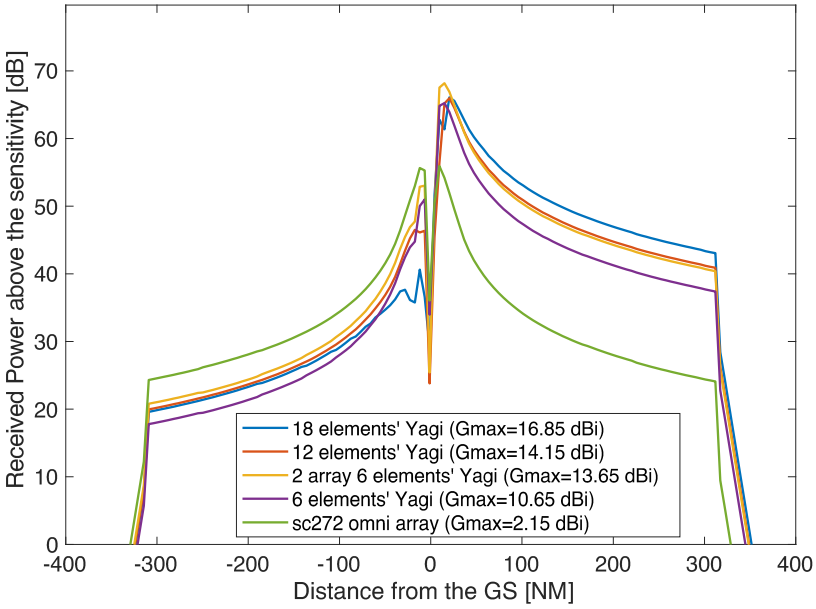

Figure 4-14: Coverage for each antennas' type when the aircraft is flying South->North (FL400).

Figure 4-14 depicts the extension of coverage when the aircraft flies at FL400. Worth noting that the aircrafts can fly even above that height.

Table 4.3: Comparison between the maximum distance for each antenna's type for FL245 and FL400.

Antennas	**G_{max} [dBi]**	**Maximum Distance Covered**				**Improvement [%]**
		FL 245		**FL 400**		
		d [km]	**d [NM]**	**d [km]**	**d [NM]**	
SC272 omni array	2.15	515	278	610	329	
6 elements' Yagi	10.65	543	293	645	348	5,78%
Two Array Yagi 6	13.65	549	296	647	349	6,07%
12 elements' Yagi	14.15	551	298			
18 elements' Yagi	16.85	555	299	653	352	6,99%

Finally, Table 4.3 compares the covered ray length for when the aircraft is flying at FL245 and FL400. Most of the traffic flows above the TMA and, for that reason, it is the most concerning area to be covered. For this thesis, it was considered the antenna with greater gains – Yagi 18 elements' antenna – however, and since the difference of maximum extension distances between the Yagi 18 elements' and the 6 elements' one differs only by 4 NM, which is not really significant, the 6 elements' Yagi could be also considered, since it has the advantage of being a smaller antenna.

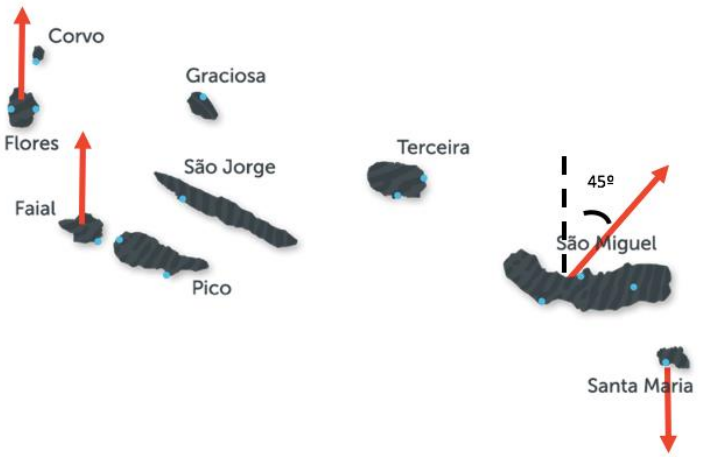

Figure 4-15: Direction of orientation of the 18 elements' Yagi antennas in the GSs (adapted from [38]).

In a way of covering more area, and since the Santa Maria GS and the one in São Miguel are close to each other, the antenna in Santa Maria was pointed to the south in order to cover a larger area. Also, to increase the coverage area even more, since the Faial GS covers a great part of the same area as the one by the GS in S. Miguel, it was evaluated whether the covered would be increased in case of rotating the antenna horizontally to East. Concluding, the best way was to rotate horizontally 45º to east the antenna set in São Miguel, and the coverage expand (Figure 4-15). Santa Maria is located south S. Miguel, and it would not benefit to point the Santa Maria's GS also in the North direction. Also, the Yagi in Porto Santo covers the East part and all the other GSs cover west. Therefore, Santa Maria's GS if pointed south, can increase the coverage area above the TMA.

When close or beyond the radio horizon, the vertical/polar angle θ_{GS} is close to 90º. Therefore, there is no need to tilt the antenna vertically, since the concern of this thesis is to cover areas beyond the horizon.

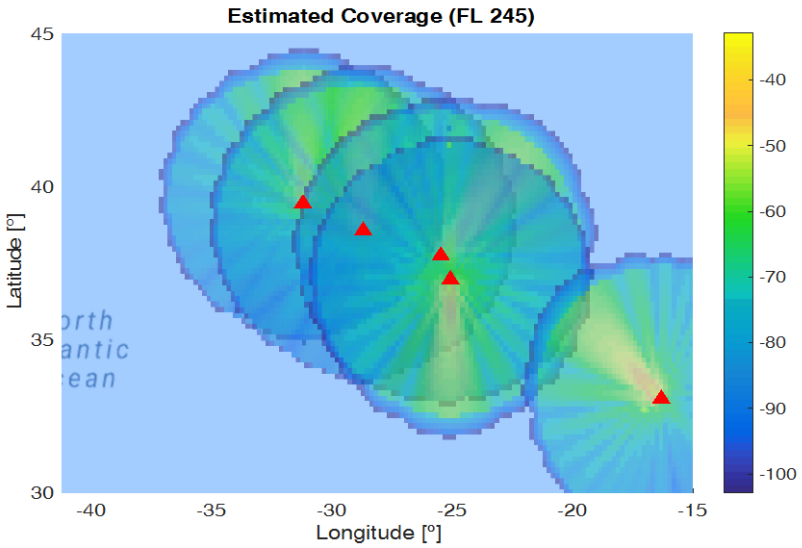

Figure 4-16: Propagation coverage area when using Yagi 18 elements' antennas in the GS (FL245).

Figure 4-16 portrays the new estimated coverage when using Yagi 18 elements' antennas at the same place as the one described in Table 4.1.

To conclude, using (3.19) to compare the coverage area (A_{cov}=2 366 400 km² ≈ 689050 NM²) with the total area in Azores' oceanic FIR gives a percentage of 46.05%, which, comparing with the one already implemented, has an expansion of ΔA= 68 000 km² = 19 800 NM², representing +2.96%.

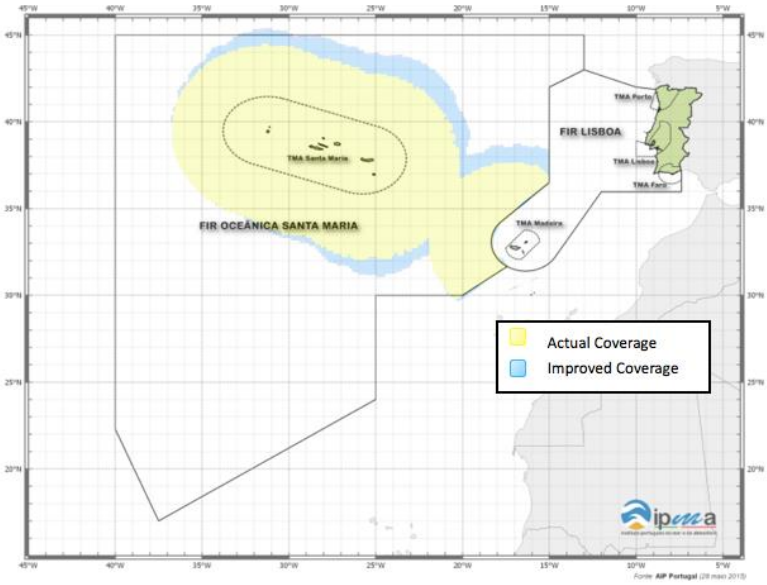

Figure 4-17: Comparison between the improved and the actual coverages.

Table 4.4: Comparison between the current and the improved coverage area.

Current Estimated Total Coverage Area	**2 298 400 km²**	**669 250 NM²**	**Improvement of 2.96 %**
Improved Estimated Total Coverage Area	2 366 400 km²	689 05 NM²	
Area Extension	68 000 km²	19 800 NM²	
Maximum distance extension	40 km	21.6 NM	Improvement of 7.77%

In addition, even though NAV currently does not use more than 3 frequencies, a study of the coverage using 4 frequencies can also be interesting.

Figure 4-18: 18 elements' Yagi directions of orientation for the 4-frequency system (adapted from [38]).

Getting another 18 elements' Yagi in Flores and in Faial, both pointed out to southwest SW (halfway between south and east) increases coverage in that direction compared with the one in Figure 4-16.

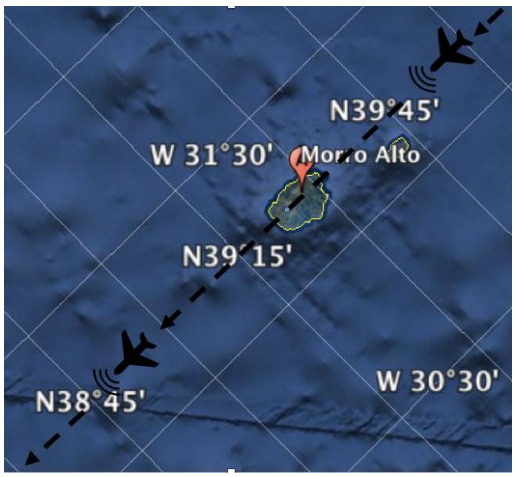

Figure 4-19: Testing aircraft's route from NE heading SW for the Morro Alto, Flores, Ground Station.

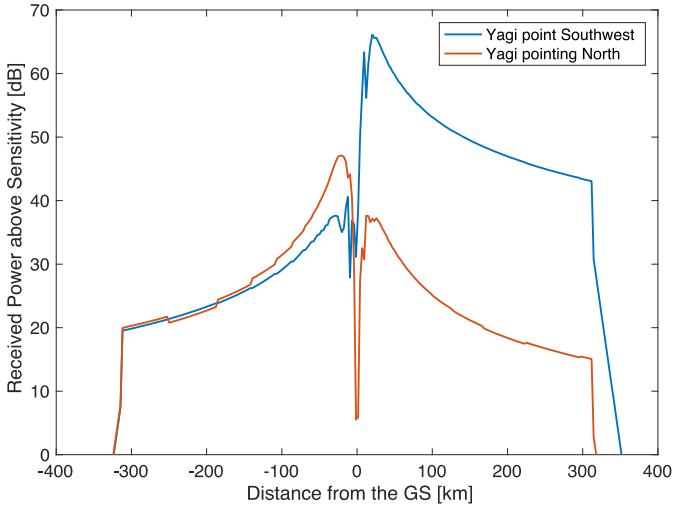

Figure 4-20: Comparison of coverage maximum distances when the aircraft's route goes from NE to SW using 18 elements' Yagi pointing north and pointing SW.

Finally, the total covered area of all 7 antennas (5 antennas covering the area portrayed in Figure 4-16 and the 2 new antennas) is illustrated in Figure 4-21. The new total coverage area is of 701 979 NM². Comparing with the solution with 5 GSs, it is an increase of area of 1.88% and with the current of 4.89%.

Table 4.5: Total coverage improvement for 4-frequency system.

Current Estimated Total Coverage Area [NM²]	**669 250**	**Improvement of 4.89%**
Improved Estimated Total Coverage Area [NM²]	701 979	
Area Extension [NM²]	32 728	

To reduce interference, the new antenna added to Morro Alto, Flores can work at the same frequency as the one in S. Miguel, since these two ground station don't have overlapping areas and the forth frequency band links to the new antenna in Cabeço Gordo, Faial.

Since 2% is not a significant improvement, and since setting new antennas translate in adding more ground controllers, this solution does not represent a priority.

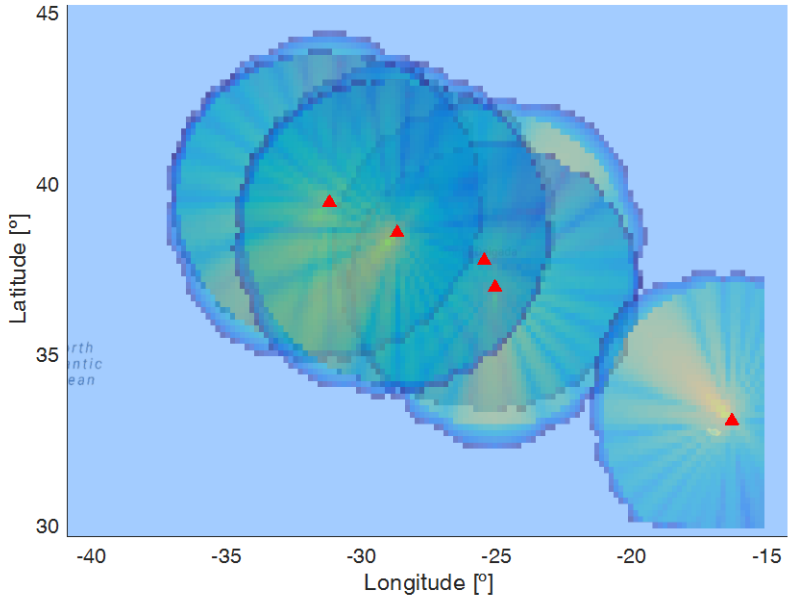

Figure 4-21: Coverage in case of having 4 working frequencies.

4.3 Antennas' Dimension

The Skymasts antennas used for this study are not defined for the Airband. Therefore, it is necessary to define the dimensions of the 18 elements' Yagi proposed in this thesis to improve the coverage area and facilitate the communication for bigger distances between the pilot and the controller.

Because Yagi antennas have been extensively analysed and experimentally tested, the process basically consists in looking at the table published in "Yagi Antenna Design" by P Viezbicke from the National Bureau of Standards [39], 1968.

As described in the 18 elements' Yagi datasheet in Annex A.6, the length of the antenna for 300 MHz is typically 3.2 m, which is really close to the one obtained in [39]. Therefore, if the distance between the reflector and the driven element as well as the distance between directors is 0.2λ, then, for 18 elements, the approximately boom length is about to 3.4λ. Note that "boom" is the long element that the directors, reflectors and feed elements are physically attached to, and dictates the length of the antenna.

Since it has to work for the whole Airband, 118 MHz, i.e. the larger wavelength must be considered. Thus, the estimated boom length comes around 8.65 m long. The length of all the elements is deployed in

Table 4.6.

Table 4.6: Reflector and directors' dimensions for the 18 elements' Yagi in the Airband.

Element	Length [m]	Element	Length [m]
Reflector	1.22	**Director 9**	0.981
Director 1	1.068	**Director 10**	0.981
Director 2	1.035	**Director 11**	0.981
Director 3	1.012	**Director 12**	0.981
Director 4	1.002	**Director 13**	0.981
Director 5	0.992	**Director 14**	0.981
Director 6	0.981	**Director 15**	0.981
Director 7	0.981	**Director 16**	0.981
Director 8	0.981		

As for a 6 elements' Yagi, one must consider the boom length as 1.2 wavelengths, i.e., 3.05 m long. As already discussed before, since this antenna is much smaller and with similar results, this antenna can be also a good suggestion.

Table 4.7: Reflector and directors' dimensions for the 6 elements' Yagi in the Air band.

Element	Length [m]
Reflector	1.22
Director 1	1.08
Director 2	1.067
Director 3	1.067
Director 4	1.08

Chapter 5

Conclusions

This chapter finalizes this work, summarizing conclusions and pointing out aspects to be developed in future work.

In domestic airspace, flight information is typically transmitted and received using VHF and UHF voice radio whereas their propagation is limited by the radio horizon. Places not covered by either VHF or UHF must be covered by HF radio and/or by SATVOICE something that is very expensive.

A typical omnidirectional antenna, in high altitudes, normally is enough to cover the aircrafts until close to the radio horizon. However, near the radio-horizon, the curvature of the Earth turns itself into an obstacle and the received power decreases drastically and the received power is not enough for the communication to be successful. Therefore, in order to extend the signal beyond that, ones could increase the transmitting power or the gains of the GS antenna as well as the aircrafts'. However, it is not practical to change all the antennas in all the airborne and most of the time it is useless to increase the transmitting power of the GS, because even though the signal is strong enough for the controller to communicate with the pilot, the pilot may not be capable of communicating with the controller. Vice-versa can also happen, when the aircraft is close to the antenna. So only the radiation pattern of the GS antenna can be practical to change. For that reason, a model considering the propagation models, antennas' radiation patterns and their locations, using directional antennas and multi-frequency systems is proposed and implemented in a simulator, conceding an estimation of the coverage area. Following, one recaps the five chapters in this thesis.

Chapter 1 gives the motivations and the ambitions for this thesis, as well as an introduction to the content in the next sections. The chapter starts with the history of communications between pilot and controller, how rudimental it was, and follows with the organization and changes in the structure for aeronautical communications. It ends with the reasons to improve the aeronautical voice communication in VHF.

As for the Chapter 2, one presents the basic concepts regarding systems and mechanisms under study. First, there is a concise introduction on how the communication between pilot and controller really works, as well as the brief description of the air band and communication voice channels and modulation. Thereafter, an overview of the propagation models for short and long distances is provided, together with a study on the different type of antennas relevant for the extension of communications. This chapter ends with a brief presentation on the state of the art in this area of study, where one presents cases from a company (Park Air Systems) that already implemented some 20 over-the-horizon VHF systems around the world, and one by ICAO in order to improve the coverage area in the Bengal Sea, India.

Chapter 3 presents all the theoretical expressions to achieve the goals of this work. It starts with a succinct analysis of the theoretical model offering an overview of its objectives and assumptions. The aircraft's position is defined in geographic coordinates so, in order to obtain the distance between the two terminals, there is the need to use some mathematical expressions.

Afterwards, one gives a detailed description of the developed model with detailed flowcharts showing the explanation of the algorithms used in the simulator, related to signal propagation, which allow to calculate the path loss caused by either the decay throughout a path or obstacles. For long distances, the main propagation mechanisms in VHF are the free space path loss model until the radio horizon and the diffraction through Earth's Curvature and Tropospheric Scattering after that. However, close to the GS there must be a special attention to the profile of the terrain, which can cause some additional attenuation on the signal. This possible extra attenuation is evaluated by the Fresnel's Ellipsoid Model,

Digital Elevation Model, Effective Earth's Radius Model, Knife-Edge and Deygout Methods. Then, there is a study of how radiation patterns vary with the relate position of the terminals, as well as a brief study of the aircrafts' antennas. At the end of the chapter, a successful assessment of the established theoretical foundations and correctly implementation of the simulator is presented.

Finally, Chapter 4 begins with the description of the location of the 5 current GSs given by NAV Portugal and their altitudes, including the terrain profile. It is worth noting that some of these locations are not the actual real ones installed, but the ones NAV Portugal suggested to be considered. The coverage area given by the simulator is considered as the real one, and it is the one that is analysed and improved.

NAV Portugal only has omnidirectional antennas limited to the radio horizon, so directional antennas were analysed. Yagi antennas are very widely used as a high-gain antenna in VHF, whose maximum gain increases with the number of driven elements. Therefore, 6, 12 and 18 elements Yagi received powers are analysed when the path length increases. As expected, the 18 elements' Yagi covers a larger distances, and it is the one that it is proposed at the end of this work.

Another aspect that should be paid attention is whether there is any interference for longer distances. NAV Portugal's advice is to consider only three frequencies to be taken into consideration. Therefore, Faial's GS antenna needs to have an operating frequency band different from the one in Flores as well as the one in S. Miguel. Santa Maria's GS antenna and the S. Miguel's cannot have the same working frequency band. So, in order to reduce interference, Faial's and Santa Maria's GS antennas can operate with the same frequency band and Faial's and S. Miguel's need to be different from the other two.

Also, there was not the need to change the location of the antennas, since they are located in high mountainous areas with almost no obstructions.

Close to the Azores' TMA, the aircrafts are obliged to fly at FL245, which is considered the worst-case scenario. Of course, when far from the TMA, aircrafts fly at FL300 or even higher which means more coverage for longer distances. Hence, one analysed the FL245 and FL400 cases. Hence, 18 elements' Yagi extends in the direction of maximum propagation about 6.99% comparing with the SC272 omnidirectional array with 2.5 dBi of gain.

The majority of the traffic flows in the upper part of the FIR; thus, one must prioritize that area. For that reason, replacing the all the antennas with 18 elements' Yagi ones, pointing North was the first experiment. Of course, since the GS in Santa Maria is near and south to the one in S. Miguel, it is more beneficial for it to be pointed South, expanding the area also in the south of Santa Maria. Also, by observation, if S. Miguel is rotated 45º East, the total coverage area also increases, since a big part of the coverage above S. Miguel is also covered by the ones in Santa Maria and Faial's. With an initial coverage of 46.05% of the FIR, there is an improvement of 2.96% comparing with the current coverage area.

However, the extension of the coverage is not the only thing that improves. Another important feature of using more directive antennas is the fact that for distances close to the horizon the received power is greater. Comparing these Yagi antennas with the SC272 omnidirectional one, near the horizon, the received power elevates more than 10 dB, i.e., ten times more.

For this thesis, the antenna with greater gains was considered – Yagi 18 elements' antenna – however, and since the difference of maximum extension distances between the Yagi 18 elements' and the 6 elements' one differs only by 4 NM, which is not really significant, the 6 elements' Yagi can be also considered, since it is a smaller antenna.

In case of using 4-frequency systems, it is then possible to improve the coverage area below the TMA, adding one antenna in Morro Alto, Flores, and other in Cabeço Gordo, Faial, pointing southwest increasing 1.88% of the covered area when comparing with the 3-frequency system and of 4.89% of the total coverage. However, 2% is not a significant improvement, therefore, it is not worth implementing these two antennas since it translates in more ground controller.

Annex

Antennas’ Datasheets

A.1 Sinclair’s Omnidirectional Array SC6172

The SC6172(E2712) antennas are fabricated using lightweight rugged components to insure easy installation while providing superior resistance to harsh environmental conditions. The SC6172(E2712) is a single feed cable version. These antennas provide reliable omnidirectional coverag. For more information go to [40].

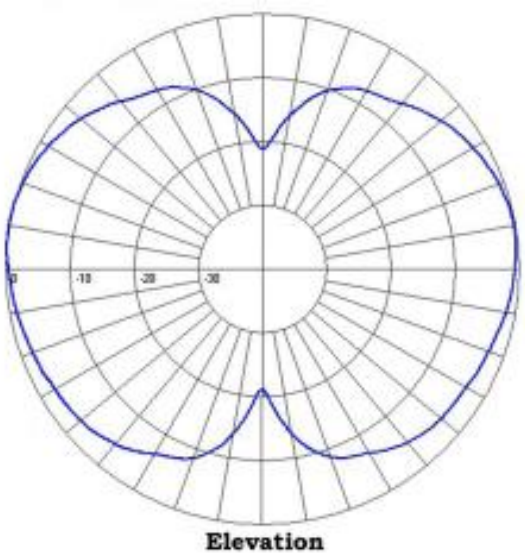

Figure A.1: Sinclair’s omnidirectional array SC6172 elevation pattern (extracted from [40]).

Table A.1: Sinclair's Omnidirectional Array SC6172 Specifications (extracted from [40]).

Frequency Range	**18-137 MHz**
Input Impedance	50 Ω
Typical Bandwidth	19 MHz
VSWR	2:1
F/B Ratio	15 dB
Maximum Input Power	250 W
Polarization	Vertical
Nominal Gain	-1.1 dBd
Vertical Beamwidth	75º

A.2 Sinclair's Omnidirectional Array SC272

The SC272 is a lightweight, collinear antenna constructed of high strength fiberglass with an aluminium coaxial skirt and base pipe. The combined features of light weight, unity gain, and low cost make this antenna a natural choice for moderate ground station antenna requirements. Mounting clamps are provided for parallel mounting to a minimum 1.9-inch diameter support pipe. For more information go to [40].

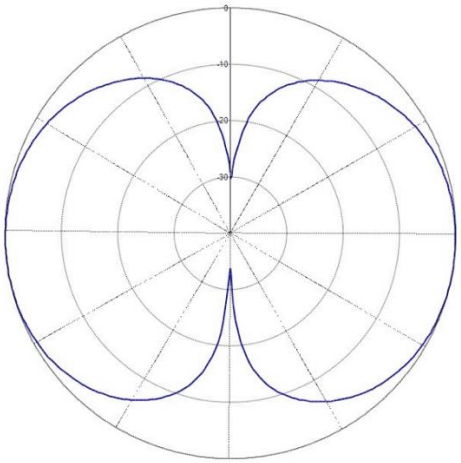

Figure A.2: Sinclair's Omnidirectional SC272 Array Elevation Pattern (extracted from [40]).

Table A.2: Sinclair's Omnidirectional Array SC272 Specifications (extracted from [40]).

Frequency Range	**18-137 MHz**
Input Impedance	50 Ω
Typical Bandwidth	19 MHz
VSWR	2:1
F/B Ratio	15 dB
Maximum Input Power	250 W
Polarization	Vertical
Nominal Gain	0 dBd
Vertical Beamwidth	85º

A.3 Skymasts' 3 elements Yagi Datasheet

The S.3Y Series are of a rugged and reliable construction for communication networks at both VHF & UHF. The one piece folded dipole incorporates a d.c. short to minimise static interference. These antennas give a gain of 6dBd with front to back ratio typically 15 dB.

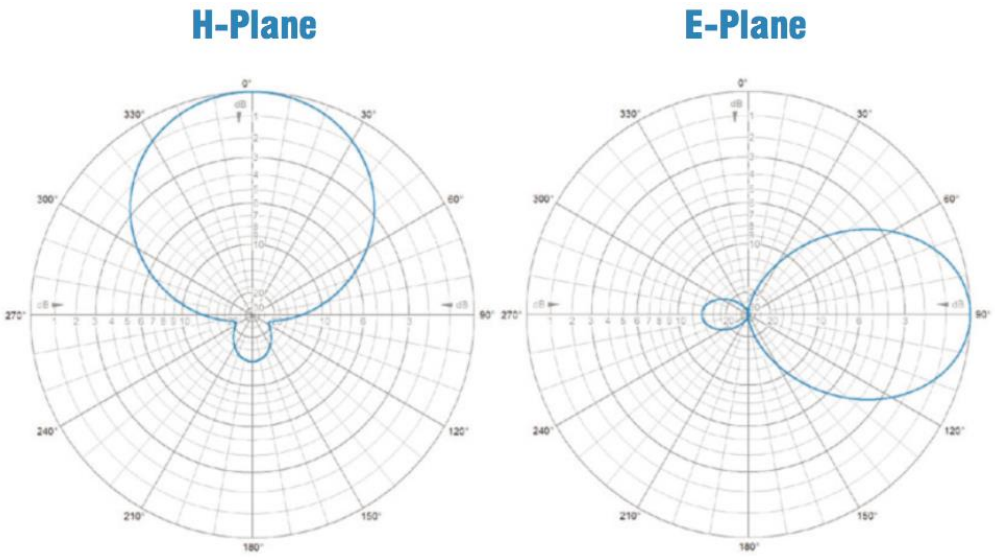

Figure A.3 :3 elements Yagi Antenna's Free Space Radiation Patterns (extracted from [34]).

Table A.3: 3 elements Yagi Antenna's Specifications (extracted from [34]).

Frequency Range	**Manufactured between 68-500 MHz**
Input Impedance	50 Ω
Typical Bandwidth	±6% of centre frequency
VSWR	<1.5:1
F/B Ratio	15 dB
Maximum Input Power	150 W
Polarization	Vertical & Horizontal
Forward Gain	6 dBd
3 dB Beamwidth	E plane 62º
	H plane 84º
Elements	19.1 mm dia. x 1.6 mm wall Al. alloy 6063T6
Support Boom	31.7 mm dia. x 2.6 mm wall Al. alloy grade 6082T6
Typical Weight	4.5 kg
Typical Length	2.2 m
Typical Wind Loading @ 45 M/S	240 N

A.4 Skymasts' 6 elements' Yagi Datasheet

The S.6Y Series are of a rugged and reliable construction for communication networks at both VHF & UHF. These antennas give a gain of 8.5dBd with front to back ratio typically 16 dB.

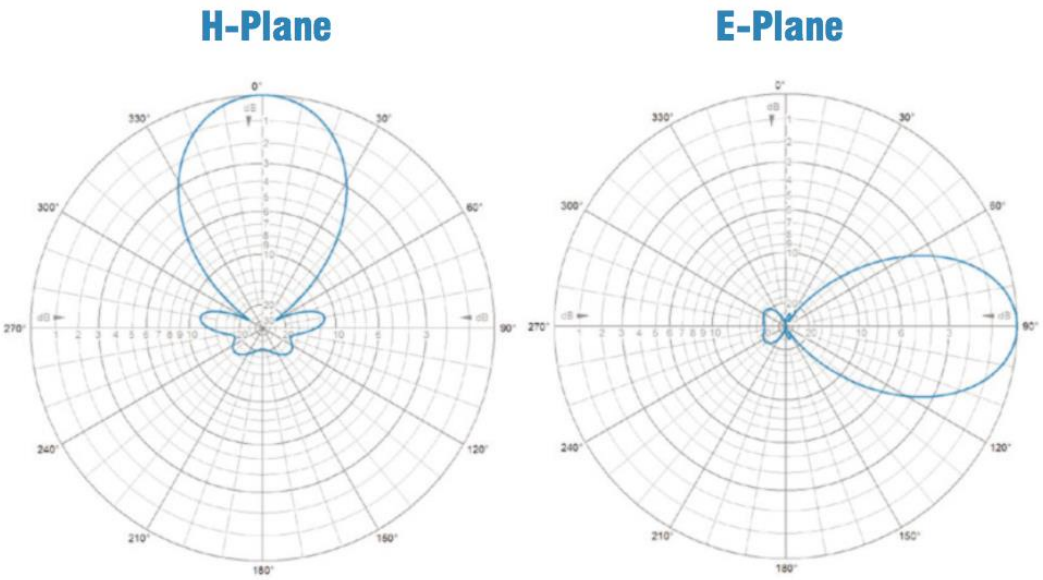

Figure A.4: 6 elements Yagi Antenna's Free Space Radiation Patterns (extracted from [35]).

Table A.4: 6 elements Yagi Antenna's Specifications (extracted from [35]).

Frequency Range	**Manufactured between 88-500 MHz**
Input Impedance	50 Ω
Typical Bandwidth	±5% of centre frequency
VSWR	<1.5:1
F/B Ratio	16 dB
Maximum Input Power	150 W
Polarization	Vertical & Horizontal
Forward Gain	8.5 dBd
3 dB Beamwidth	E plane 56º
	H plane 63º
Elements	19.1 mm dia. x 1.6 mm wall Al. alloy 6063T6
Support Boom	31.7 mm dia. x 2.6 mm wall Al. alloy grade 6082T6
Typical Weight	6 kg @ 125 MHz
Typical Length	3.055 m @ 125 MHz
Typical Wind Loading @ 45 M/S	208 N

A.5 Skymasts' 12 elements' Yagi Datasheet

The S.12Y Series offer high gain from a highly directive radiation pattern for use in UHF link systems. The one piece folded dipole incorporates a d.c. short to minimise static interference. These antennas give a gain of 12dBd with front to back ratio typically 20dB.

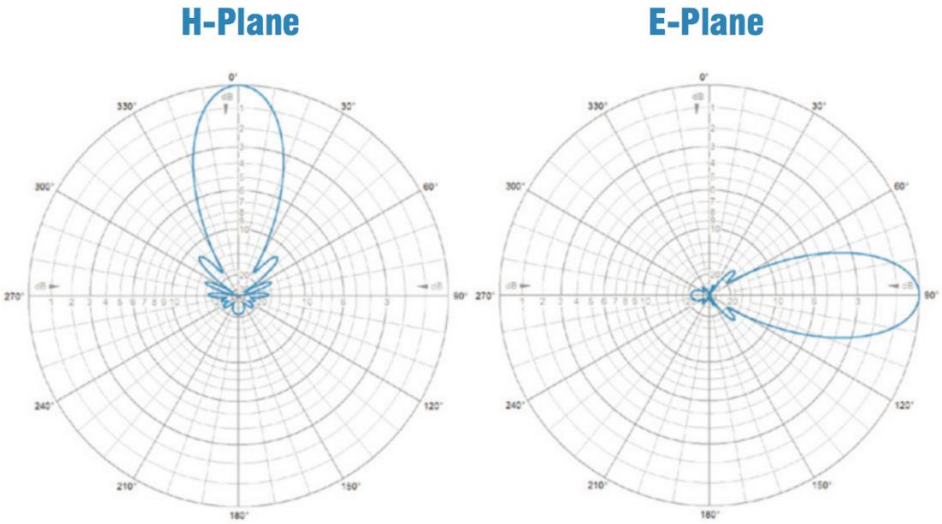

Figure A.5: 12 elements Yagi Antenna's Free Space Radiation Patterns (extracted from [36]).

Table A.5: 12 elements Yagi Antenna's Specification (extracted from [36]).

Frequency Range	**Manufactured between 300-500 MHz**
Input Impedance	50 Ω
Typical Bandwidth	±4% of centre frequency
VSWR	<1.5:1
F/B Ratio	20 dB
Maximum Input Power	150 W
Polarization	Vertical & Horizontal
Forward Gain	12 dBd
3 dB Beamwidth	E plane 34º
	H plane 40º
Elements	12.7 mm dia. x 1.6 mm wall Al. alloy 6063T6
Support Boom	31.7 mm dia. x 2.6 mm wall Al. alloy grade 6082T6
Typical Weight	4.5 kg
Typical Length	2.5 m
Typical Wind Loading @ 45 M/S	150 N

A.6 Skymasts' 18 elements' Yagi Datasheet

The S.18Y series offer high gain from a highly directive radiation pattern for use in UHF link systems gain together with a four elements' reflector giving high protection from unwanted signals. These antennas give a gain of 14.7dBd with front to back ratio typically 25dB.

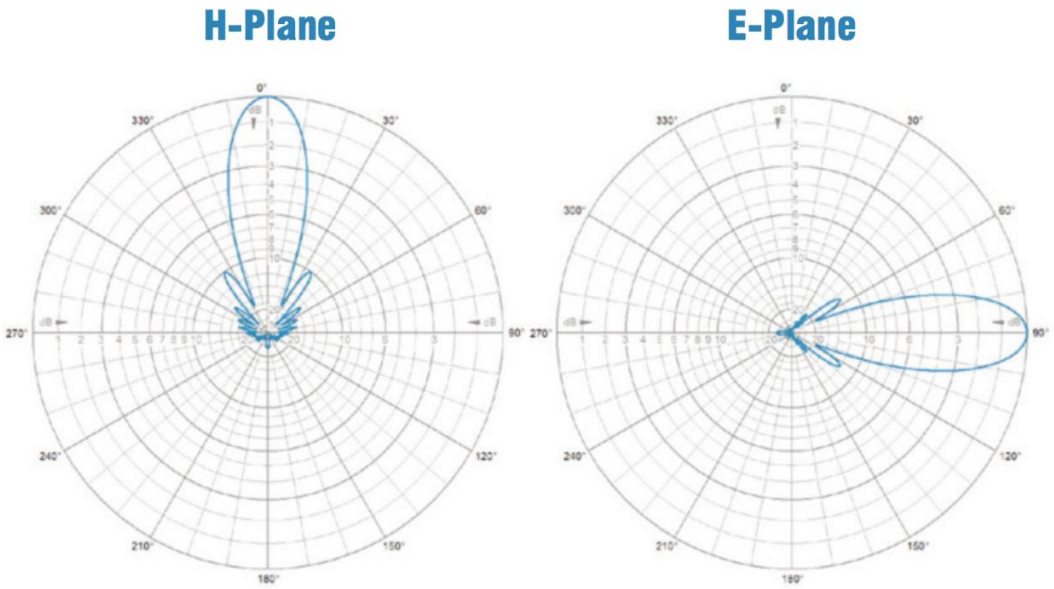

Figure A.6: 18 elements Yagi Antenna's Free Space Radiation Patterns (extracted from [37]).

Table A.6: 18 elements Yagi Antenna's Specifications (extracted from [37]).

Frequency Range	**Manufactured between 300-500 MHz**
Input Impedance	50 Ω
Typical Bandwidth	±4% of centre frequency
VSWR	<1.5:1
F/B Ratio	25 dB
Maximum Input Power	150 W
Polarization	Vertical & Horizontal
Forward Gain	14.7 dBd
3 dB Beamwidth	E plane 24º
	H plane 32º
Elements	12.7 mm dia. x 1.6 mm wall Al. alloy 6063T6
Support Boom	31.7 mm dia. x 2.6 mm wall Al. alloy grade 6082T6
Typical Weight	7 kg
Typical Length	3.2 m
Typical Wind Loading @ 45 M/S	248 N

References

[1] Nolan, M., *Fundamentals of Air Traffic Control*, Purdue University, USA 2011.

[2] LDACS, Future aeronautical communications, http://www.ldacs.com/about-ldacs1/background-and-motivation/

[3] NAV PORTUGAL E.RE, https://www.nav.pt/en/nav/air-navigation-services-1/aeronautical-infrastructure/control-centres

[4] Portuguese Institute for Sea and Atmosphere, https://www.ipma.pt/en/enciclopedia/aeronautica/index.html?page=firs.xml, May. 2015

[5] Federal Aviation Administration*, North Atlantic Operations and Airspace Manual*, NAT Doc 007, ICAO European and North Atlantic Office (https://www.faa.gov/air_traffic/separation_standards/rvsm/documents/NAT_Doc_007_V-2016-1.pdf)

[6] Stacey,D., *Aeronautical Radio Communication Systems and Networks*, John Wiley & Sons, Ltd, 2008.

[7] Malvern, A., *Improvements to VHF air-to-ground communication*, British Airspace

[8] Trippe J., Gao, X., *Amplitude Modulated Radio Applications in Aviation*, Project Report, Vanderbilt University, 2012.

[9] *8.33 kHz Channel spacing- What is this?,* Roger-Wilco- the first air traffic management blog, http://www.roger-wilco.net/8-33-khz-channel-spacing-%E2%80%93-what-is-this/, Mar. 2010

[10] Correia, L.M., *Propagation Models*, Lecture Notes of Mobile Communication Systems, IST/UL, Lisbon, Portugal, 2014.

[11] Santos R., *Impact of FM Broadcast Signals on Aeronautical Radionavigation*, M.Sc. Thesis, Instituto Superior Tecnico, Technical University of Lisbon, Lisbon, Portugal, Feb 2015

[12] ITU, “Propagation prediction techniques and data required for the design of trans-horizon radio-relay systems”, *Recommendation ITU-R* P.617-3, ITU, Switzerland, 2013.

[13] ITU, “Propagation by diffraction”, *Recommendation ITU-R* P.526-13, ITU, Switzerland, 2013.

[14] Rodrigues,A.J. and Sanguino,J.E., *Hertzian Beams – Formulary (in Portuguese), Course Material of Radio Telecommunication Systems*, IST/UL, Lisbon, Portugal, 2014.

[15] Everyday VHF, UHF, and SHF propagation. http://www.qsl.net/oz1rh/troposcatter99/troposcatter99.htm

[16] ITU, “Effects of tropospheric refraction on radiowave propagation”, *Recommendation ITU-R* P.834-836, ITU, Switzerland, 2007.

[17] Hitney, H.V and Vieth, R, *Statistical Assessment of Evaporation Duct Propagation, IEEE Transactions on Antennas and Propagation*, Vol 38, No. 6, June 1990

[18] Mufti N., *Investigation into the effects of the troposphere on VHF and UHF radio propagation and interference between co-frequency fixe links,* M.Sc Thesis, University of Leicester, UK, 2011.

[19] ITU,“The radio refractive index: Its formula and refractivity data”*, Recommendation ITU-R* P.341-345, ITU, Switzerland, 2003.

[20] *Quarter wave ground antenna*, Amateur radio station MM0ZIF- training zone antennas*,* http://www.mm0zif.org.uk/training-zone/antennas/14-wave-ground-plane-antenna/

[21] Pool I., *Yagi Antenna,* Radio-Electronics – Resources and analysis for electronic engineers, *http://www.radio-electronics.com/info/antennas/yagi/yagi.php*

[22] Moreira,A., Linear Antennas (in Portuguese), Lecture Notes of Antennas, IST/UL, Lisbon, Portugal, 2014.

[23] Marsh G., *Longer Legs for VHF*, Avionics Magazine*,* Mar.2004 (http://www.aviationtoday.com/av/air-traffic-control/Longer-Legs-for-VHF_780.html)

[25] Correia, L.M., *Antennas for bases and mobiles*, Lecture Notes of Mobile Communication Systems, IST/UL, Lisbon, Portugal, 2014.

[26] Bower A., Chandler D., “Extended Range VHF Communications improve performance of air transport operations”, *ICAO Journal*, Vol.57, No.3, Nov.2002, pp.23 and pp.31

[27] Northrop Grumman Group, https://www.northropgrummaninternational.com/northrop-grumman-to-supply-extended-range-air-traffic-communications-to-curacao/ , Jun. 2013

[28] ICAO, “VHF coverage over Idian Airspace”, *Eight Meeting of the Communications /Navigation /Surveillance and Meteorology Sub-Group (CNS/MET SG/8) of APANPIRG,* Thailand, Jul.2004, https://www.icao.int/Meetings/AMC/MA/2004/CNSMET_SG8/ip20.pdf

[29] Airports Authority of India, “Air Traffic Flow Management –India”, http://us-indiaacp.com/downloads/seminars/atfm/ATFM_ACP.pdf

[30] Costa T., *Analysis of Aircraft Accuracy Location in Aeronautical Multilateration Systems*, M.Sc. Thesis, Instituto Superior Tecnico, Technical University of Lisbon, Lisbon, Portugal, April 2017.

[31] ICAO, Annex 10 - Aeronautical Telecommunications, Vol. 3, No. 2, Montreal, Canada, Jul. 2017.

[32] NASA LP DAAC, Global Data Explorer, http://gdex.cr.usgs.gov/gdex/, Sep. 2016.

[33] Gil, F., Claro, A., Ferreira, J., Pardelinha, C. and Correia, L.M., "A 3-D Interpolation Method for Base-Station Antenna Radiation Patterns", *IEEE Antennas and Propagation Magazine*, 43, 2, Apr 2001

[34] Skymasts, 3 elements' Yagi datasheet, http://www.skymasts.com/products/view/three-element-yagi-antenna

[35] Skymasts, 6 elements' Yagi datasheet, http://www.skymasts.com/products/view/six-element-yagi-antenna

[36] Skymasts, 12 elements' Yagi datasheet, http://www.skymasts.com/products/view/twelve-element-yagi-antenna

[37] Skymasts, 18 elements' Yagi datasheet, http://www.skymasts.com/products/view/eighteen-element-yagi-antenna

[38] Azores Archipelogue, https://www.azoreschoice.com/azores/

[39] National Bureau of Standards, "Yagi Antenna Design", NBS technical note 688, US department of commerce, Dec. 1976, http://tf.nist.gov/general/pdf/451.pdf

[40] Sinclair Technologies, Antenna's Manufacteurer, http://www.sinclairtechnologies.com/catalog/group.aspx?id=2&market=12